



HAL
open science

The Actin Depolymerizing Factor StADF2 Alters StREM1.3 Plasma Membrane Nanodomains to Inhibit the Virus X

Marie-Dominique Jolivet, Paul Gouguet, Anthony Legrand, Kaltra Xhelilaj, Natalie Faiss, Aurélie Massoni-Laporte, Terezinha Robbe, Isabelle Sagot, Marie Boudsocq, Sylvie German-Retana, et al.

► **To cite this version:**

Marie-Dominique Jolivet, Paul Gouguet, Anthony Legrand, Kaltra Xhelilaj, Natalie Faiss, et al.. The Actin Depolymerizing Factor StADF2 Alters StREM1.3 Plasma Membrane Nanodomains to Inhibit the Virus X. 2025. hal-04833207

HAL Id: hal-04833207

<https://cnrs.hal.science/hal-04833207v1>

Preprint submitted on 17 Jan 2025

HAL is a multi-disciplinary open access archive for the deposit and dissemination of scientific research documents, whether they are published or not. The documents may come from teaching and research institutions in France or abroad, or from public or private research centers.

L'archive ouverte pluridisciplinaire **HAL**, est destinée au dépôt et à la diffusion de documents scientifiques de niveau recherche, publiés ou non, émanant des établissements d'enseignement et de recherche français ou étrangers, des laboratoires publics ou privés.



Distributed under a Creative Commons Attribution 4.0 International License

1 **TITLE: The actin depolymerizing factor StADF2 alters StREM1.3 plasma membrane**
2 **nanodomains to inhibit the *Potato Virus X***

3

4 **AUTHORS:** Marie-Dominique Jolivet^{1*}, Paul Gouguet^{1,2*}, Anthony Legrand^{1,3,7}, Kaltra Xhelilaj²,
5 Natalie Faiss², Aurélie Massoni-Laporte⁴, Terezinha Robbe¹, Isabelle Sagot⁴, Marie Boudsocq⁵,
6 Sylvie German-Retana⁶, Suayib Üstün², Antoine Loquet³, Birgit Habenstein³, Véronique
7 Germain^{1§}, Sébastien Mongrand^{1§}, Julien Gronnier^{1,2\$,#}

8

9 **AFFILIATIONS**

10 1, Laboratoire de Biogenèse Membranaire (LBM) UMR-5200, CNRS-Univ. Bordeaux, F-33140
11 Villenave d'Ornon, France

12 2, Zentrum für Molekularbiologie der Pflanzen (ZMBP), Eberhard Karls Universität Tübingen,
13 Auf der Morgenstelle 32, 72076 Tübingen, Germany

14 3, Institute of Chemistry & Biology of Membranes & Nanoobjects (UMR5248 CBMN), IECB,
15 CNRS, Université Bordeaux, Institut Polytechnique Bordeaux, Pessac, France

16 4, IBGC - Institut de biochimie et génétique cellulaires (IBGC) UMR-5095. CNRS-Univ.
17 Bordeaux. 146 rue Léo Saignat, 33077 Bordeaux

18 5, Institute of Plant Sciences Paris-Saclay (IPS2), Université Paris-Saclay, CNRS, INRAE, Univ
19 Evry, Université Paris Cité 91190 Gif-sur-Yvette, France.

20 6, UMR 1332 Biologie du Fruit et Pathologie, INRAE Université Bordeaux, 71 Av. E. Bourlaux,
21 CS20032, CEDEX, 33882 Villenave d'Ornon, France.

22 7, Current address: Loschmidt Laboratories, Department of Experimental Biology and
23 RECETOX, Faculty of Science, Masaryk University, Brno, Czech Republic.

24

25 *, These authors (M-D. J, P.G.) contributed equally to the work and should be considered as
26 co-first authors.

27 §, These authors (V.G, S.M., J.G.) contributed equally to the work and should be considered
28 as co-last authors.

29 #, Corresponding author: Julien Gronnier <julien.gronnier@zmbp.uni-tuebingen.de> Zentrum
30 für Molekularbiologie der Pflanzen (ZMBP), Eberhard Karls Universität Tübingen, Auf der
31 Morgenstelle 72076, Tübingen, Germany.

32

33 **ABSTRACT**

34 The dynamic regulation of the plasma membrane (PM) organization at the nanoscale
35 emerged as a key element shaping the outcome of host-microbe interactions. Protein
36 organization into nanodomains (ND) is often assumed to be linked to the activation of cellular
37 processes. In contrast, we have previously shown that the phosphorylation of the *Solanum*
38 *tuberosum* REM1.3 (StREM1.3) N-terminal domain disperses its native ND organization and
39 promotes its inhibitory effect on *Potato Virus X* (PVX) cell-to-cell movement. Here, we show
40 that the phosphorylation of StREM1.3 modify the chemical environment of numerous
41 residues in its intrinsically-disordered N-terminal domain. We leveraged exploratory screens
42 to identify potential phosphorylation-dependent interactors of StREM1.3. Herewith, we
43 uncovered uncharacterized regulators of PVX cell-to-cell movement, linking StREM1.3 to
44 autophagy, water channels and the actin cytoskeleton. We show that the *Solanum tuberosum*
45 actin depolymerizing factors 2 (StADF2) alters StREM1.3 NDs and limits PVX cell-to-cell
46 movement in a REMORIN-dependent manner. Mutating a conserved single residue reported
47 to affect ADFs affinity to actin inhibits StADF2 effect on StREM1.3 ND organization and PVX
48 cell-to-cell movement. These observations provide functional links between the organization
49 of plant PM and the actin cytoskeleton and suggests that the alteration of StREM1.3 ND
50 organization promotes plant anti-viral responses. We envision that analogous PM re-
51 organization applies for additional signaling pathways in plants and in other organisms.

52

53 **INTRODUCTION**

54 The plasma membrane (PM) actively hosts, modulates and coordinates a myriad of signaling
55 events essential to the development and survival of all living organisms. Across the tree of
56 life, PM lipids and proteins have been found to be dynamically organized into diverse
57 nanoscopic environments termed nanodomains (NDs) (Gronnier et al., 2018; Jacobson et al.,
58 2019; Lopez & Koch, 2017; Malinsky et al., 2013). NDs have been proposed to provide
59 dedicated biochemical and biophysical environments to ensure acute, specific and robust
60 signaling events (Kusumi et al., 2012; Sezgin et al., 2017). In plants, emerging evidence suggest
61 that ND formation and integrity rely on the intimate interplay between lipids, proteins, the
62 cell wall and the cytoskeleton (Galindo-Trigo et al., 2020; Gronnier et al., 2018, 2019; Jaillais
63 & Ott, 2020). The molecular events underlying context-dependent PM re-organization and
64 their functional consequences remain largely unknown.

65 REMORINs are structural components of the PM playing regulatory functions in plant-microbe
66 interactions and hormone signaling (reviewed in Gouguet et al., 2021). REMORINs of different
67 groups (Raffaele et al., 2007) tend to form distinct and coexisting NDs proposed to regulate
68 specific signaling pathways (Bücherl et al., 2017; Jarsch et al., 2014). The molecular bases for
69 REMORINs ND organization are best characterized for group 1 REMORINs (Gronnier et al.,
70 2018; Jaillais & Ott, 2020). Group 1 REMORINs NDs are proposed to be liquid-ordered and
71 enriched in sterols and saturated lipids (Demir et al., 2013; Gronnier et al., 2017; Mamode
72 Cassim et al., 2019; Raffaele et al., 2009). Their native organization is dictated by direct
73 interactions with anionic phospholipids (Gronnier et al., 2017; Legrand et al., 2019; Legrand
74 et al., 2022; Perraki et al., 2012), and can be modulated by post-translational modifications
75 such as S-acylation (Fu et al., 2018; Konrad et al., 2014) and phosphorylation (Perraki et al.,
76 2018). Group 1 REMORINs regulate cell-to-cell movement of viruses belonging to diverse
77 genus (Cheng et al., 2020; Fu et al., 2018; Huang et al., 2019; Raffaele et al., 2009; Rocher et
78 al., 2022). Notably, their function in hindering *Potexviruses*, to which the *Potato Virus X* (PVX)
79 belongs, is conserved in *Nicotiana benthamiana*, *Solanum lycopersicum* and *Arabidopsis*
80 *thaliana* (Abel et al., 2021; Perraki et al., 2018; Perraki et al., 2014; Raffaele et al., 2009),
81 suggesting an ancestral function conserved across at least 100 million years of evolution.
82 Most REMORINs bear a predicted intrinsically-disordered N-terminal domain found to be
83 phosphorylated in multiple plant species and across a wide range of physiological conditions
84 (Gouguet et al., 2021). Phosphorylation affects the chemistry, structure, and conformational
85 ensemble of intrinsically-disordered domains (IDD), and consequently their association with
86 protein partners (Mukhopadhyay et al., 2022; Wright & Dyson, 2014). In view of their PM ND
87 organization, their ability to homo-oligomerize, and their putative IDD, REMORINs have been
88 proposed to act as scaffolds. Here, we show that the N-terminal domain of StREM1.3 is
89 intrinsically disordered and that its phosphorylation modifies the chemical environment of
90 numerous residues. Leveraging yeast two-hybrid screens, we identified interactors of a
91 phosphomimic variant of StREM1.3 and uncovered uncharacterized regulators of PVX
92 infection. We show that the *Solanum tuberosum* actin depolymerizing factors 2 (StADF2)
93 alters StREM1.3 NDs and limits PVX propagation in a REMORIN-dependent manner. We
94 observed that StADF2 activity is affected by mutating a conserved residue regulating ADFs
95 affinity to actin. Altogether, these observations suggest that active modulation of REMORIN
96 ND organization promotes plant anti-viral responses.

97 **RESULTS**

98 ***StREM1.3 N-terminal domain is intrinsically disordered and its phosphorylation leads to***
99 ***changes in the chemical environment of numerous residues.***

100 We previously showed that phosphorylation of the *Solanum tuberosum* REMORIN1.3
101 (StREM1.3) N-terminal domain regulates its ND organization and function (Perraki et al.,
102 2018). Notably, using photoactivated localization microscopy, we observed that a
103 phosphomimic form of StREM1.3, StREM1.3^{S74D T86D S91D} (further referred to as StREM1.3^{DDD})
104 which restricts PVX cell-to-cell movement, presented a dispersed organization (Perraki et al.,
105 2018). We confirmed this observation using laser scanning confocal microscopy (Figure 1A).
106 However, the molecular bases underlying StREM1.3 ND dispersion remain unknown.
107 StREM1.3 N-terminal domain is predicted to be intrinsically disordered (Marín et al., 2012;
108 Perraki et al., 2018). We used liquid-state NMR spectroscopy to characterize the properties
109 of StREM1.3 N-terminal domain. ¹H-¹⁵N HMQC spectra of untagged StREM1.3¹⁻¹¹⁶ purified in
110 native and denaturing conditions (Figure S1A) both displayed a narrow $\delta(1H)$ distribution
111 (between ~ 7.5 - 8.5 ppm, Figure S1B), demonstrating that StREM1.3 N-terminal domain is
112 intrinsically disordered.

113 We then asked how phosphorylation modulates StREM1.3 N-terminal domain. The
114 *Arabidopsis thaliana* calcium-dependent protein kinase 3 (AtCPK3) was previously shown to
115 phosphorylate group 1 REMORINs (Mehlmer et al., 2010; Perraki et al., 2018) and to restrict
116 PVX cell-to-cell movement in a REMORIN-dependent manner (Perraki et al., 2018). Liquid-
117 state NMR spectroscopy showed that the addition of AtCPK3, which phosphorylates
118 StREM1.3 N-terminal domain *in vitro* (Legrand et al., 2022; Perraki et al., 2018) (Figure S2),
119 induced chemical shift perturbations on several residues without altering the intrinsically
120 disordered nature of StREM1.3¹⁻¹¹⁶ (Figures 1B and 1C). The chemical shifts of the amide
121 groups are very sensitive to the local chemical environment of the concerned residues. These
122 observations indicate the modification of the chemical environment for multiple residues
123 induced by phosphorylation which may modulate StREM1.3 intra- and intermolecular
124 interactions. We therefore hypothesized that the phosphorylation of StREM1.3 intrinsically
125 disordered N-terminal domain may modulate its association with specific protein partners to
126 inhibit PVX cell-to-cell movement.

127

128 **A StREM1.3 phosphomimic-based yeast two hybrid exploratory screen identifies**
129 **uncharacterized regulators of PVX cell-to-cell movement.**

130 To identify proteins which may associate with StREM1.3 in a phosphorylation-dependent
131 manner, we used exploratory split-ubiquitin yeast two-hybrid (SUY2H) screens comparing WT
132 and phosphomimic variant of StREM1.3, StREM1.3^{DDD}. First, we tested whether StREM1.3 was
133 a functional bait in SUY2H. We observed that expression of Cub-StREM1.3^{WT} or Cub-
134 StREM1.3^{DDD} did not lead to autoactivation and that StREM1.3 self-association (Bariola et al.,
135 2004.; Martinez et al., 2019; Perraki et al., 2014) could be resolved in this system, indicating
136 that both Cub-StREM1.3 or Cub-StREM1.3^{DDD} were functional in SUY2H assays (Figure S3A and
137 S3B). Further, we observed that GFP-tagged StREM1.3 and StREM1.3^{DDD} localized to the PM
138 when expressed in yeast (Figure S3C). Interestingly, both proteins formed PM domains in
139 yeast (Figure S3C), suggesting that StREM1.3^{DDD} dispersed organization as observed in *N.*
140 *benthamiana* (Figure 1A) is conditioned by plant factors.

141 To enrich for relevant factors during viral infection, we generated a cDNA library using mRNA
142 extracted from both PVX-infected and healthy *N. benthamiana* leaf epidermis (Figure S4A and
143 S4B). We used peeled epidermis to limit the occurrence of chloroplastic proteins in our screen
144 as previously reported (Bernard et al., 2012). We confirmed the presence of PVX:GFP in the
145 infected epidermis by confocal microscopy (Figure S4C). Side-by-side screens of this library by
146 SUY2H revealed an approximate 6-fold increase in the number of positive clones obtained
147 with StREM1.3^{DDD} compared to StREM1.3 (Figures 2A, 2B and 2C), suggesting that the
148 phosphomimic form of StREM1.3 has an increased ability to generate protein-protein
149 interactions. Sequencing of the clones presenting reliable interaction identified 37 and 140
150 distinct proteins for StREM1.3 and StREM1.3^{DDD} respectively (Figure 2D and supplemental
151 table 1). Among them, only 6 proteins were identified in both screens (Figure 2D) suggesting
152 that StREM1.3 and StREM1.3^{DDD} have largely distinct interactomes. Among identified proteins
153 are orthologs of Arabidopsis 14-3-3 and HYPERSENSITIVE INDUCED REACTION proteins which
154 have been previously shown to associate with group 1 REMORINs (Huang et al., 2019; Lv et
155 al., 2017), pointing toward the functional relevance of the identified proteins. To further
156 explore the role of REM interactors in PVX infection, we prioritized candidates based on the
157 number of clones identified in SUY2H screen, their co-purification and/or co-expression with
158 Arabidopsis REMs in omics studies and cloned them as translational fusions with the HA
159 epitope-tag for functional studies. Among the 10 candidates tested in PVX:GFP cell-to-cell

160 propagation assays (Figures 3A and 3B), the expression of 7 candidates impaired PVX
161 propagation: the Plasma membrane intrinsic protein 1C (NbPIP1C), Delta tonoplast integral
162 protein (NbTIP2;1), Thioredoxin superfamily protein 4 (NbTRX4), Metallothionein 2B
163 (NbMT2B), Calreticulin 3 (NbCRT3), Autophagy 8i (NbATG8i) and Actin Depolymerizing Factor
164 3 (NbADF3) (Figure 3B, Figure S5). Altogether, these observations both suggest that the
165 phosphorylation of StREM1.3 promotes its association with specific proteins to limit PVX cell-
166 to-cell movement and link plant response to PVX with the autophagy pathway and water
167 channels notably.

168

169 **StADF2 affects StREM1.3 nanodomains and inhibits PVX cell-to-cell movement in a**
170 **REMORIN-dependent manner.**

171 Among the genes tested, the *N. benthamiana* actin depolymerizing factor (ADF) 3 (NbADF3,
172 NbS00025994g0001.1) was one of the most potent in limiting PVX cell-to-cell movement
173 (Figure 3B). To corroborate the potential implication of an ADF-REMORIN module involved in
174 response to PVX, we first tested the ability of an ortholog of NbADF3 from *Solanum tuberosum*
175 (StADF2, Soltu.DM.04G007350) to associate with StREM1.3. Co-immunoprecipitation
176 experiments, using transient expression in *N. benthamiana* leaves, showed that StADF2 and
177 StREM1.3 associate *in planta* (Figure 4A). We next tested whether StADF2 limits PVX infection.
178 Using group 1 REMORINs knock-down stable transgenic *N. benthamiana* lines (hpREM #1.4
179 and #10.2; Perraki et al., 2018), we observed that the transient overexpression of StADF2
180 limited PVX cell-to-cell movement in a REMORIN-dependent manner (Figure 4B, 4C). These
181 results indicate that ADFs and REMORINs cooperate to limit PVX infection. Because the ND
182 organization of the *Arabidopsis thaliana* REM1.2 and of the *Medicago truncatula* SYMBIOTIC
183 REMORIN (SYMREM; MtREM2.2) rely on the integrity of the actin cytoskeleton (Liang et al.,
184 2018; Szymanski et al., 2015) and that the active form of StREM1.3 correlates with a disperse
185 PM organization (Figure 1A; Perraki et al., 2018), we wondered whether StADF2 could
186 regulate StREM1.3 ND organization to inhibit PVX. We observed that overexpression of
187 StADF2 affected YFP-StREM1.3 ND organization (Figures S6A and S6B), suggesting that
188 StREM1.3 ND organization relies on actin cytoskeleton integrity. In good agreement,
189 cytochalasin D treatment, which inhibits actin polymerization, was sufficient to affect YFP-
190 StREM1.3 ND organization (Figures S6C and S6D). The affinity of ADFs for actin is decreased
191 by their phosphorylation on a conserved N-terminally located Serine (Figure S7; Augustine et

192 al., 2008; Dong & Hong, 2013; Y. J. Lu et al., 2020; Porter et al., 2012; Ressad et al., 1998).
193 Interestingly, we observed that replacing the corresponding Serine residue by an Aspartic acid
194 in StADF2 (StADF^{S6D}) altered its ability to modify StREM1.3 ND organization (Figures 5A and
195 5B) and to restrict PVX cell-to-cell movement (Figure 5C and 5D). Altogether, these data
196 indicate that StADF2 restricts PVX cell-to-cell movement by actively modulating actin
197 cytoskeleton and REMORINs ND organization.

198

199 **DISCUSSION**

200 How processes are regulated in space and time within the plasma membrane (PM) remains
201 largely obscure. In plants, REMORINs are structural elements of the PM emerging as versatile
202 regulatory components of various signaling pathways in plant development and plant-
203 microbe interactions (Gui et al., 2016; Kohorn et al., 2016; Liang et al., 2018; Perraki et al.,
204 2014). This functional versatility is suspected to be encoded in their variable and intrinsically
205 disordered N-terminal domain (Gouguet et al., 2021). REMORINs IDD have been found to be
206 poly-phosphorylated in many plant species and across a wide range of physiological
207 conditions (Gouguet et al., 2021). Here we show that the phosphorylation of StREM1.3 IDD
208 modifies the chemical environment at the level of the protein backbone which may operate
209 as a molecular switch in regulating its association with specific partners. In good agreement,
210 we observed that a phosphomimic variant of StREM1.3 has both an increased ability to
211 generate protein-protein interaction and a distinct interactome from the wild-type protein in
212 yeast. These observations suggest the existence of context-dependent REMORINs phospho-
213 codes and open way toward their identification and the study of their implication in the
214 regulation of REMORINs-associated molecular complexes and signaling pathways.

215 Functional analysis of selected StREM1.3 interactors unveiled uncharacterized host regulators
216 of PVX infection (Figure 3). These observations suggest that plant immune response to PVX
217 involves the autophagy machinery (NbATG8i), water permeable channels (NbPIP1;3,
218 NbTIP2;1), regulators of cellular redox status (NbTRX4) and iron-binding proteins (NbMT2B).
219 Several orthologs of these proteins were previously linked to immunity in various plants
220 species against pathogens of several kingdoms. For instance, the autophagy machinery has
221 been found to play a central role in plant immunity against bacteria, fungi and viruses and can
222 as well be manipulated by pathogens for their own benefits (Fu et al., 2018; Hafrén et al.,
223 2018; Leary et al., 2018; Leong et al., 2022; F. Li et al., 2020; MacHaria et al., 2019; Niu et al.,

224 2021; Üstün et al., 2018; Yang et al., 2018). Altogether, these observations suggest that
225 REMORINs play a central role in regulating key cellular events in plant immunity, the definition
226 of the precise mechanisms will require further investigation.

227 NbADF3 and StADF2 belong to the subclass 1 of the ADF protein family (Inada, 2017), which
228 has been reported to be involved in multiple plant-pathogen interactions (Lu et al., 2015; Lu
229 et al., 2020; Porter et al., 2012; Porter & Day, 2013; Tian et al., 2009). Subclass 1 ADFs have
230 been identified in *Arabidopsis thaliana* plasmodesmata (PD) proteome (Brault et al., 2019),
231 which may imply that their role in restricting of PVX propagation (Figure 3B and 4C) relies on
232 a direct modulation of plasmodesmata. Further, actin disruption has been recently proposed
233 as an immune response leading to callose deposition (Leontovyčová et al., 2020) and both
234 AtADF4 and REMORINs are required for callose deposition in response to bacterial elicitors
235 (Li et al., 2012; Ma et al., 2022). Since StREM1.3 regulates callose deposition at PD (Perraki et
236 al., 2018) and that StADF2 limits PVX in a REMORIN-dependent manner (Figure 4C),
237 modulation of actin cytoskeleton and of StREM1.3 ND organization by StADF2 may underly
238 REMORIN-regulated callose accumulation at PD. Recently, evidences indicate that REMORINs
239 and the actin cytoskeleton are working hand in hand during plant-microbe interactions.
240 *Arabidopsis* REM1.2 promotes type-I Formin ND organization to foster actin nucleation in
241 response to bacterial flagellin (Ma et al., 2022) while SYMREM1-induced membrane topology
242 modifications during symbiosis depends on the actin cytoskeleton (Su et al., 2023). Our
243 observations further reinforce the tight functional interplay between REMORINs and the actin
244 cytoskeleton. Interestingly, two subclass 1 *Arabidopsis* ADFs (AtADF1 and AtADF4) as well as
245 group 1 REM were shown to be phosphorylated by AtCPK3 (Dong & Hong, 2013a; Lu et al.,
246 2020). Moreover, it was observed that CPK3 modulated actin cytoskeleton in response to
247 bacterial elicitors (Lu et al., 2020) and limited PVX cell-to-cell movement in a REMORIN-
248 dependent manner (Mehlmer et al., 2010; Perraki et al., 2018), which hints that CPK-ADF-
249 REMs may correspond to a conserved immune signaling module against invading microbes.
250 Stimuli-dependent organization of proteins in NDs is often presumed to be associated with
251 initiation and activation of cellular processes. In good agreement, the stabilization of the small
252 GTPase Rho-of-plants 6 (ROP6) into NDs upon auxin perception supports its function in
253 regulating gravitropism (Platre et al., 2019). In addition, ROP6 forms specific domains
254 promoting the production of reactive oxygen species upon osmotic stress (Smokvarska et al.,
255 2020). However, recent reports suggest that the functional interplay between PM lateral

256 organization and the functional status of its constituents is far more complex. While osmotic
257 stimulation induces ND organization of the NADPH oxidase RBOHD and of ROP6 (Smokvarska
258 et al., 2020), it concomitantly leads to an increased mobility of the aquaporin PIP2;1 and of
259 the proton pump ATPase AHA2 (Martinière et al., 2019). In yeast, the arginine permease Can1
260 accumulates into so-called membrane compartment occupied by Can1 (MCC) in its inactive,
261 substrate-free form, while its active form shows a dispersed organization within the PM
262 (Gournas et al., 2018). Similarly, substrate perception by the yeast methionine permease
263 Mup1 induces its reorganization from NDs to a disperse plasma membrane network (Busto et
264 al., 2018). We previously showed that native ND organization of StREM1.3 is required to
265 support its function in limiting PVX cell-to-cell movement (Gronnier et al., 2017). Yet, active
266 phosphomimic form of StREM1.3 presents a dispersed organization (Perraki et al., 2018;
267 Figure 1A) suggesting that StREM1.3 is activated within NDs and subsequently dispersed.
268 Here, we show that StADF2 alters StREM1.3 ND organization and limits PVX cell-to-cell
269 movement in a REMORIN-dependent manner (Figure 4). Mutating a conserved single residue
270 reported to affect ADFs affinity to actin inhibits StADF2 effect on StREM1.3 ND organization
271 and PVX cell-to-cell movement (Figure 5). Altogether, these observations suggest that active
272 modulation of actin cytoskeleton by StADF2 changes StREM1.3 nanoscale organization to
273 limit PVX cell-to-cell movement. In mammals, actin depolymerization have been shown to
274 promote B cell activation by enabling B cell antigen receptor clustering in the immune synapse
275 (Droubi et al., 2022; Mattila et al., 2016; Wang & Huse, 2022). Since REMORINs have been
276 proposed to regulate various cell-surface receptor signaling pathways (Bücherl et al., 2017;
277 Gui et al., 2016; Liang et al., 2018), a similar mechanism could apply in response to PVX and
278 in other contexts. Our study shades light on the activation of a PM-based immune response
279 by membrane scaffold dispersion. We envision that analogous mechanisms may be conserved
280 across organisms.

281

282 **REFERENCES**

- 283 Abel, N. B., Buschle, C. A., Hernandez-Ryes, C., Burkart, S. S., Deroubaix, A.-F., Mergner, J.,
284 Gronnier, J., Jarsch, I. K., Folgmann, J., Braun, K. H., Bayer, E., Germain, V., Derbyshire,
285 P., Menke, F. L. H., Kemmerling, B., Zipfel, C., Küster, B., Mongrand, S., Marín, M., &
286 Ott, T. (2021). A hetero-oligomeric remorin-receptor complex regulates plant
287 development. *BioRxiv*, 2021.01.28.428596. <https://doi.org/10.1101/2021.01.28.428596>
- 288 Augustine, R. C., Vidali, L., Kleinman, K. P., & Bezanilla, M. (2008). Actin depolymerizing
289 factor is essential for viability in plants, and its phosphoregulation is important for tip
290 growth. *The Plant Journal*, 54(5), 863–875. [https://doi.org/10.1111/J.1365-](https://doi.org/10.1111/J.1365-313X.2008.03451.X)
291 313X.2008.03451.X
- 292 Bariola, P. A., Retelska, D., Stasiak, A., Kammerer, R. A., Fleming, A., Hijri, M., Frank, S., &
293 Farmer, E. E. (n.d.). *Remorins form a novel family of coiled coil-forming oligomeric and*
294 *filamentous proteins associated with apical, vascular and embryonic tissues in plants.*
- 295 Bernard, A., Domergue, F., Pascal, S., Jetter, R., Renne, C., Faure, J. D., Haslam, R. P., Napier,
296 J. A., Lessire, R., & Joubès, J. (2012). Reconstitution of Plant Alkane Biosynthesis in
297 Yeast Demonstrates That Arabidopsis ECERIFERUM1 and ECERIFERUM3 Are Core
298 Components of a Very-Long-Chain Alkane Synthesis Complex. *The Plant Cell*, 24(7),
299 3106–3118. <https://doi.org/10.1105/TPC.112.099796>
- 300 Brault, M. L., Petit, J. D., Immel, F., Nicolas, W. J., Glavier, M., Brocard, L., Gaston, A.,
301 Fouché, M., Hawkins, T. J., Crowet, J., Grison, M. S., Germain, V., Rocher, M., Kraner,
302 M., Alva, V., Claverol, S., Paterlini, A., Helariutta, Y., Deleu, M., ... Bayer, E. M. (2019).
303 Multiple C2 domains and transmembrane region proteins (MCTP s) tether membranes
304 at plasmodesmata . *EMBO Reports*, 20(8). <https://doi.org/10.15252/embr.201847182>
- 305 Bücherl, C. A., Jarsch, I. K., Schudoma, C., Segonzac, C., Mbengue, M., Robatze, S., MacLean,
306 D., Ott, T., & Zipfe, C. (2017a). Plant immune and growth receptors share common
307 signalling components but localise to distinct plasma membrane nanodomains. *ELife*, 6,
308 1–28. <https://doi.org/10.7554/eLife.25114>
- 309 Busto, J. V, Elting, A., Haase, D., Spira, F., Kuhlman, J., Schäfer-Herte, M., & Wedlich-Söldner,
310 R. (2018). Lateral plasma membrane compartmentalization links protein function and
311 turnover. *The EMBO Journal*, 37(16). <https://doi.org/10.15252/EMBJ.201899473>
- 312 Cheng, G., Yang, Z., Zhang, H., Zhang, J., & Xu, J. (2020). Remorin interacting with PCaP1
313 impairs Turnip mosaic virus intercellular movement but is antagonised by VPg. *New*
314 *Phytologist*, 225(5), 2122–2139. <https://doi.org/10.1111/NPH.16285>
- 315 Crooks, G. E., Hon, G., Chandonia, J. M., & Brenner, S. E. (2004). WebLogo: a sequence logo
316 generator. *Genome Research*, 14(6), 1188–1190. <https://doi.org/10.1101/GR.849004>
- 317 Dagdas, Y. F., Beihaj, K., Maqbool, A., Chaparro-Garcia, A., Pandey, P., Petre, B., Tabassum,
318 N., Cruz-Mireles, N., Hughes, R. K., Sklenar, J., Win, J., Menke, F., Findlay, K., Banfield,
319 M. J., Kamoun, S., & Bozkurt, T. O. (2016). An effector of the irish potato famine
320 pathogen antagonizes a host autophagy cargo receptor. *ELife*, 5(JANUARY2016).
321 <https://doi.org/10.7554/ELIFE.10856>
- 322 Demir, F., Horntrich, C., Blachutzik, J. O., Scherzer, S., Reinders, Y., Kierszniowska, S.,
323 Schulze, W. X., Harms, G. S., Hedrich, R., Geiger, D., & Kreuzer, I. (2013). Arabidopsis
324 nanodomain-delimited ABA signaling pathway regulates the anion channel SLAH3.
325 *Proceedings of the National Academy of Sciences of the United States of America*,
326 110(20), 8296–8301. <https://doi.org/10.1073/pnas.1211667110>
- 327 Dong, C. H., & Hong, Y. (2013a). Arabidopsis CDPK6 phosphorylates ADF1 at N-terminal
328 serine 6 predominantly. *Plant Cell Reports*, 32(11), 1715–1728.

- 329 <https://doi.org/10.1007/S00299-013-1482-6>
- 330 Dong, C. H., & Hong, Y. (2013b). Arabidopsis CDPK6 phosphorylates ADF1 at N-terminal
331 serine 6 predominantly. *Plant Cell Reports*, 32(11), 1715–1728.
332 <https://doi.org/10.1007/S00299-013-1482-6/FIGURES/9>
- 333 Droubi, A., Wallis, C., Anderson, K. E., Rahman, S., de Sa, A., Rahman, T., Stephens, L.,
334 Hawkins, P. T., & Lowe, M. (2022). The inositol 5-phosphatase INPP5B regulates B cell
335 receptor clustering and signaling. *The Journal of Cell Biology*, 221(9).
336 <https://doi.org/10.1083/JCB.202112018>
- 337 Edgar, R. C. (2004). MUSCLE: multiple sequence alignment with high accuracy and high
338 throughput. *Nucleic Acids Research*, 32(5), 1792–1797.
339 <https://doi.org/10.1093/NAR/GKH340>
- 340 Escusa, S., Camblong, J., Galan, J. M., Pinson, B., & Daignan-Fornier, B. (2006). Proteasome-
341 and SCF-dependent degradation of yeast adenine deaminase upon transition from
342 proliferation to quiescence requires a new F-box protein named Saf1p. *Molecular*
343 *Microbiology*, 60(4), 1014–1025. <https://doi.org/10.1111/J.1365-2958.2006.05153.X>
- 344 Fu, S., Xu, Y., Li, C., Li, Y., Wu, J., & Zhou, X. (2018). Rice Stripe Virus Interferes with S-
345 acylation of Remorin and Induces Its Autophagic Degradation to Facilitate Virus
346 Infection. *Molecular Plant*, 11(2), 269–287.
347 <https://doi.org/10.1016/J.MOLP.2017.11.011>
- 348 Galindo-Trigo, S., Blümke, P., Simon, R., & Butenko, M. A. (2020). Emerging mechanisms to
349 fine-tune receptor kinase signaling specificity. *Current Opinion in Plant Biology*, 57, 41–
350 51. <https://doi.org/10.1016/J.PBI.2020.05.010>
- 351 Goodstein, D. M., Shu, S., Howson, R., Neupane, R., Hayes, R. D., Fazo, J., Mitros, T., Dirks,
352 W., Hellsten, U., Putnam, N., & Rokhsar, D. S. (2012). Phytozome: a comparative
353 platform for green plant genomics. *Nucleic Acids Research*, 40(D1), D1178–D1186.
354 <https://doi.org/10.1093/nar/gkr944>
- 355 Gouguet, P., Gronnier, J., Legrand, A., Perraki, A., Jolivet, M. D., Deroubaix, A. F., Retana, S.
356 G., Boudsocq, M., Habenstein, B., Mongrand, S., & Germain, V. (2021). Connecting the
357 dots: From nanodomains to physiological functions of REMORINS. In *Plant Physiology*
358 (Vol. 185, Issue 3, pp. 632–649). American Society of Plant Biologists.
359 <https://doi.org/10.1093/PLPHYS/KIAA063>
- 360 Gournas, C., Gkionis, S., Carquin, M., Twyffels, L., Tyteca, D., & André, B. (2018).
361 Conformation-dependent partitioning of yeast nutrient transporters into starvation-
362 protective membrane domains. *Proceedings of the National Academy of Sciences of the*
363 *United States of America*, 115(14), E3145–E3154.
364 <https://doi.org/10.1073/PNAS.1719462115/VIDEO-7>
- 365 Gronnier, J., Crowet, J.-M., Habenstein, B., Nasir, M. N., Bayle, V., Hosy, E., Platre, M. P.,
366 Gouguet, P., Raffaele, S., Martinez, D., Grelard, A., Loquet, A., Simon-Plas, F., Gerbeau-
367 Pissot, P., Der, C., Bayer, E. M., Jaillais, Y., Deleu, M., Germain, V., ... Mongrand, S.
368 (2017). Structural basis for plant plasma membrane protein dynamics and organization
369 into functional nanodomains. *ELife*, 6. <https://doi.org/10.7554/eLife.26404>
- 370 Gronnier, J., Gerbeau-Pissot, P., Germain, V., Mongrand, S., & Simon-Plas, F. (2018). Divide
371 and Rule: Plant Plasma Membrane Organization. In *Trends in Plant Science* (Vol. 23,
372 Issue 10, pp. 899–917). Elsevier Ltd. <https://doi.org/10.1016/j.tplants.2018.07.007>
- 373 Gronnier, J., Legrand, A., Loquet, A., Habenstein, B., Germain, V., & Mongrand, S. (2019).
374 Mechanisms governing subcompartmentalization of biological membranes. *Current*
375 *Opinion in Plant Biology*, 52, 114–123. <https://doi.org/10.1016/J.PBI.2019.08.003>

- 376 Gui, J., Zheng, S., Liu, C., Shen, J., Li, J., & Li, L. (2016). OsREM4.1 Interacts with OsSERK1 to
377 Coordinate the Interlinking between Abscisic Acid and Brassinosteroid Signaling in Rice.
378 *Developmental Cell*, 38(2), 201–213. <https://doi.org/10.1016/j.devcel.2016.06.011>
- 379 Hafrén, A., Üstün, S., Hochmuth, A., Svenning, S., Johansen, T., & Hofius, D. (2018). Turnip
380 Mosaic Virus Counteracts Selective Autophagy of the Viral Silencing Suppressor HCpro.
381 *Plant Physiology*, 176(1), 649–662. <https://doi.org/10.1104/PP.17.01198>
- 382 Huang, D., Sun, Y., Ma, Z., Ke, M., Cui, Y., Chen, Z., Chen, C., Ji, C., Tran, T. M., Yang, L., Lam,
383 S. M., Han, Y., Shu, G., Friml, J., Miao, Y., Jiang, L., & Chen, X. (2019). Salicylic acid-
384 mediated plasmodesmal closure via Remorin-dependent lipid organization.
385 *Proceedings of the National Academy of Sciences of the United States of America*,
386 116(42), 21274–21284. <https://doi.org/10.1073/pnas.1911892116>
- 387 Inada, N. (2017). Plant actin depolymerizing factor: actin microfilament disassembly and
388 more. *Journal of Plant Research*, 130(2), 227–238. [https://doi.org/10.1007/s10265-](https://doi.org/10.1007/s10265-016-0899-8)
389 016-0899-8
- 390 Jacobson, K., Liu, P., & Lagerholm, B. C. (2019). The Lateral Organization and Mobility of
391 Plasma Membrane Components. In *Cell* (Vol. 177, Issue 4, pp. 806–819). Cell Press.
392 <https://doi.org/10.1016/j.cell.2019.04.018>
- 393 Jaillais, Y., & Ott, T. (2020). The nanoscale organization of the plasma membrane and its
394 importance in signaling: A proteolipid perspective. *Plant Physiology*, 182(4), 1682–
395 1696. <https://doi.org/10.1104/PP.19.01349>
- 396 Jarsch, I. K., Konrad, S. S. A., Stratil, T. F., Urbanus, S. L., Szymanski, W., Braun, P., Braun, K.
397 H., & Ott, T. (2014). Plasma membranes are Subcompartmentalized into a plethora of
398 coexisting and diverse microdomains in Arabidopsis and Nicotiana benthamiana. *Plant*
399 *Cell*, 26(4), 1698–1711. <https://doi.org/10.1105/tpc.114.124446>
- 400 Karimi, M., Inzé, D., & Depicker, A. (2002). GATEWAY vectors for Agrobacterium-mediated
401 plant transformation. *Trends in Plant Science*, 7(5), 193–195.
402 [https://doi.org/10.1016/S1360-1385\(02\)02251-3](https://doi.org/10.1016/S1360-1385(02)02251-3)
- 403 Kohorn, B. D., Hoon, D., Minkoff, B. B., Sussman, M. R., & Kohorn, S. L. (2016). Rapid oligo-
404 galacturonide induced changes in protein phosphorylation in arabidopsis. *Molecular*
405 *and Cellular Proteomics*, 15(4), 1351–1359. <https://doi.org/10.1074/mcp.M115.055368>
- 406 Konrad, S. S. A., Popp, C., Stratil, T. F., Jarsch, I. K., Thallmair, V., Folgmann, J., Marín, M., &
407 Ott, T. (2014). S-acylation anchors remorin proteins to the plasma membrane but does
408 not primarily determine their localization in membrane microdomains. *New*
409 *Phytologist*, 203(3), 758–769. <https://doi.org/10.1111/nph.12867>
- 410 Kusumi, A., Fujiwara, T. K., Chadda, R., Xie, M., Tsunoyama, T. A., Kalay, Z., Kasai, R. S., &
411 Suzuki, K. G. N. (2012). Dynamic organizing principles of the plasma membrane that
412 regulate signal transduction: commemorating the fortieth anniversary of Singer and
413 Nicolson’s fluid-mosaic model. *Annual Review of Cell and Developmental Biology*, 28,
414 215–250. <https://doi.org/10.1146/ANNUREV-CELLBIO-100809-151736>
- 415 Leary, A. Y., Sanguankiatichai, N., Duggan, C., Tumtas, Y., Pandey, P., Segretin, M. E.,
416 Salguero Linares, J., Savage, Z. D., Yow, R. J., & Bozkurt, T. O. (2018). Modulation of
417 plant autophagy during pathogen attack. *Journal of Experimental Botany*, 69(6), 1325–
418 1333. <https://doi.org/10.1093/JXB/ERX425>
- 419 Legrand, A., G.-Cava, D., Jolivet, M.-D., Decossas, M., Lambert, O., Bayle, V., Jaillais, Y.,
420 Loquet, A., Germain, V., Boudsocq, M., Habenstein, B., Tirado, M. V., & Mongrand, S.
421 (2022). Structural determinants of REMORIN nanodomain formation in anionic
422 membranes. *Biophysical Journal*. <https://doi.org/10.1016/J.BPJ.2022.12.035>

- 423 Legrand, A., Martinez, D., Grélard, A., Berbon, M., Morvan, E., Tawani, A., Loquet, A.,
424 Mongrand, S., & Habenstein, B. (2019). Nanodomain Clustering of the Plant Protein
425 Remorin by Solid-State NMR. *Frontiers in Molecular Biosciences*, 6.
426 <https://doi.org/10.3389/fmolb.2019.00107>
- 427 Leong, J. X., Raffener, M., Spinti, D., Langin, G., Franz-Wachtel, M., Guzman, A. R., Kim, J.-G.,
428 Pandey, P., Minina, A. E., Macek, B., Hafr En, A., Bozkurt, T. O., Mudgett, M. B., Börnke,
429 F., Hofius, D., Suayib, &, & Ust€ Un, €.. (2022). A bacterial effector counteracts host
430 autophagy by promoting degradation of an autophagy component. *The EMBO Journal*,
431 41(13), e110352. <https://doi.org/10.15252/EMBJ.2021110352>
- 432 Leontovychová, H., Kalachova, T., & Janda, M. (2020). Disrupted actin: a novel player in
433 pathogen attack sensing? *The New Phytologist*, 227(6), 1605–1609.
434 <https://doi.org/10.1111/NPH.16584>
- 435 Li, F., Zhang, M., Zhang, C., & Zhou, X. (2020). Nuclear autophagy degrades a geminivirus
436 nuclear protein to restrict viral infection in solanaceous plants. *The New Phytologist*,
437 225(4), 1746–1761. <https://doi.org/10.1111/NPH.16268>
- 438 Li, J., Henty-Ridilla, J. L., Huang, S., Wang, X., Blanchoin, L., & Staigera, C. J. (2012). Capping
439 protein modulates the dynamic behavior of actin filaments in response to phosphatidic
440 acid in arabidopsis. *Plant Cell*, 24(9), 3742–3754.
441 <https://doi.org/10.1105/TPC.112.103945/DC1>
- 442 Liang, P., Stratil, T. F., Popp, C., Marín, M., Folgmann, J., Mysore, K. S., Wen, J., & Ott, T.
443 (2018). Symbiotic root infections in *Medicago truncatula* require remorin-mediated
444 receptor stabilization in membrane nanodomains. *Proceedings of the National
445 Academy of Sciences of the United States of America*, 115(20), 5289–5294.
446 <https://doi.org/10.1073/pnas.1721868115>
- 447 Lopez, D., & Koch, G. (2017). Exploring functional membrane microdomains in bacteria: an
448 overview. *Current Opinion in Microbiology*, 36, 76–84.
449 <https://doi.org/10.1016/J.MIB.2017.02.001>
- 450 Lu, L., Wu, G., Xu, X., Luan, H., Zhi, H., Cui, J., Cui, X., & Chen, X. (2015). Soybean actin-
451 depolymerizing factor 2 interacts with Soybean mosaic virus-encoded P3 protein. *Virus
452 Genes*, 50(2), 333–339. <https://doi.org/10.1007/s11262-014-1150-0>
- 453 Lu, Y. J., Li, P., Shimono, M., Corrión, A., Higaki, T., He, S. Y., & Day, B. (2020).
454 Arabidopsis calcium-dependent protein kinase 3 regulates actin cytoskeleton
455 organization and immunity. *Nature Communications*, 11(1).
456 <https://doi.org/10.1038/s41467-020-20007-4>
- 457 Lv, X., Jing, Y., Xiao, J., Zhang, Y., Zhu, Y., Julian, R., & Lin, J. (2017). Membrane microdomains
458 and the cytoskeleton constrain AtHIR1 dynamics and facilitate the formation of an
459 AtHIR1-associated immune complex. *The Plant Journal*, 90(1), 3–16.
460 <https://doi.org/10.1111/TPJ.13480>
- 461 Ma, Z., Sun, Y., Zhu, X., Yang, L., Chen, X., & Miao, Y. (2022). Membrane nanodomains
462 modulate formin condensation for actin remodeling in Arabidopsis innate immune
463 responses. *The Plant Cell*, 34(1), 374–394. <https://doi.org/10.1093/PLCELL/KOAB261>
- 464 MacHaria, M. W., Tan, W. Y. Z., Das, P. P., Naqvi, N. I., & Wong, S. M. (2019). Proximity-
465 dependent biotinylation screening identifies NbHYPK as a novel interacting partner of
466 ATG8 in plants. *BMC Plant Biology*, 19(1). <https://doi.org/10.1186/S12870-019-1930-8>
- 467 Malinsky, J., Opekarová, M., Grossmann, G., & Tanner, W. (2013). Membrane
468 microdomains, rafts, and detergent-resistant membranes in plants and fungi. In *Annual
469 Review of Plant Biology* (Vol. 64, pp. 501–529). Annu Rev Plant Biol.

- 470 <https://doi.org/10.1146/annurev-arplant-050312-120103>
- 471 Mamode Cassim, A., Gouguet, P., Gronnier, J., Laurent, N., Germain, V., Grison, M., Boutté,
472 Y., Gerbeau-Pissot, P., Simon-Plas, F., & Mongrand, S. (2019). Plant lipids: Key players of
473 plasma membrane organization and function. In *Progress in Lipid Research* (Vol. 73, pp.
474 1–27). Elsevier Ltd. <https://doi.org/10.1016/j.plipres.2018.11.002>
- 475 Marín, M., Thallmair, V., & Ott, T. (2012). The intrinsically disordered N-terminal region of
476 AtREM1.3 remorin protein mediates protein-protein interactions. *Journal of Biological*
477 *Chemistry*, 287(47), 39982–39991. <https://doi.org/10.1074/jbc.M112.414292>
- 478 Martin, K., Kopperud, K., Chakrabarty, R., Banerjee, R., Brooks, R., & Goodin, M. M. (2009).
479 Transient expression in *Nicotiana benthamiana* fluorescent marker lines provides
480 enhanced definition of protein localization, movement and interactions in planta. *The*
481 *Plant Journal*, 59(1), 150–162. <https://doi.org/10.1111/J.1365-313X.2009.03850.X>
- 482 Martinez, D., Legrand, A., Gronnier, J., Decossas, M., Gouguet, P., Lambert, O., Berbon, M.,
483 Verron, L., Grélard, A., Germain, V., Loquet, A., Mongrand, S., & Habenstein, B. (2019).
484 Coiled-coil oligomerization controls localization of the plasma membrane REMORINs.
485 *Journal of Structural Biology*, 206(1), 12–19. <https://doi.org/10.1016/j.jsb.2018.02.003>
- 486 Martinière, A., Fiche, J. B., Smokvarska, M., Mari, S., Alcon, C., Dumont, X., Hematy, K.,
487 Jaillais, Y., Nollmann, M., & Maurel, C. (2019). Osmotic stress activates two reactive
488 oxygen species pathways with distinct effects on protein nanodomains and diffusion.
489 *Plant Physiology*, 179(4), 1581–1593. <https://doi.org/10.1104/pp.18.01065>
- 490 Mattila, P. K., Batista, F. D., & Treanor, B. (2016). Dynamics of the actin cytoskeleton
491 mediates receptor cross talk: An emerging concept in tuning receptor signaling. *The*
492 *Journal of Cell Biology*, 212(3), 267–280. <https://doi.org/10.1083/JCB.201504137>
- 493 Mehlmer, N., Wurzinger, B., Stael, S., Hofmann-Rodrigues, D., Csaszar, E., Pfister, B., Bayer,
494 R., & Teige, M. (2010). The Ca²⁺-dependent protein kinase CPK3 is required for MAPK-
495 independent salt-stress acclimation in *Arabidopsis*. *Plant Journal*, 63(3), 484–498.
496 <https://doi.org/10.1111/j.1365-313X.2010.04257.x>
- 497 Mukhopadhyay, S., Newcombe, E. A., Delaforge, E., Hartmann-Petersen, R., Skriver, K., &
498 Kragelund, B. B. (2022). How phosphorylation impacts intrinsically disordered proteins
499 and their function. *Essays in Biochemistry*, 66(7), 901–913.
500 <https://doi.org/10.1042/EBC20220060>
- 501 Nakagawa, T., Kurose, T., Hino, T., Tanaka, K., Kawamukai, M., Niwa, Y., Toyooka, K.,
502 Matsuoka, K., Jinbo, T., & Kimura, T. (2007). Development of series of gateway binary
503 vectors, pGWBs, for realizing efficient construction of fusion genes for plant
504 transformation. *Journal of Bioscience and Bioengineering*, 104(1), 34–41.
505 <https://doi.org/10.1263/JBB.104.34>
- 506 Niu, E., Liu, H., Zhou, H., Luo, L., Wu, Y., Andika, I. B., & Sun, L. (2021). Autophagy Inhibits
507 Intercellular Transport of Citrus Leaf Blotch Virus by Targeting Viral Movement Protein.
508 *Viruses*, 13(11). <https://doi.org/10.3390/V13112189>
- 509 Perraki, A., Gronnier, J., Gouguet, P., Boudsocq, M., Deroubaix, A.-F., Simon, V., German-
510 Retana, S., Legrand, A., Habenstein, B., Zipfel, C., Bayer, E., Mongrand, S., & Germain, V.
511 (2018). REM1.3's phospho-status defines its plasma membrane nanodomain
512 organization and activity in restricting PVX cell-to-cell movement. *PLoS Pathogens*,
513 14(11). <https://doi.org/10.1371/journal.ppat.1007378>
- 514 Perraki, A., Binaghi, M., Mecchia, M. A., Gronnier, J., German-Retana, S., Mongrand, S.,
515 Bayer, E., Zelada, A. M., & Germain, V. (2014). StRemorin1.3 hampers Potato virus X
516 TGBp1 ability to increase plasmodesmata permeability, but does not interfere with its

- 517 silencing suppressor activity. *FEBS Letters*, 588(9), 1699–1705.
518 <https://doi.org/10.1016/j.febslet.2014.03.014>
- 519 Perraki, Artemis, Cacas, J. L., Crowet, J. M., Lins, L., Castroviejo, M., German-Retana, S.,
520 Mongrand, S., & Raffaele, S. (2012). Plasma membrane localization of *Solanum*
521 *tuberosum* Remorin from group 1, homolog 3 is mediated by conformational changes
522 in a novel C-terminal anchor and required for the restriction of potato virus X
523 movement. *Plant Physiology*, 160(2), 624–637. <https://doi.org/10.1104/pp.112.200519>
- 524 Platre, M. P., Bayle, V., Armengot, L., Bareille, J., del Mar Marquès-Bueno, M., Creff, A.,
525 Maneta-Peyret, L., Fiche, J. B., Nollmann, M., Miège, C., Moreau, P., Martinière, A., &
526 Jaillais, Y. (2019). Developmental control of plant Rho GTPase nano-organization by the
527 lipid phosphatidylserine. *Science*, 364(6435), 57–62.
528 <https://doi.org/10.1126/science.aav9959>
- 529 Porter, K., & Day, B. (2013). Actin branches out to link pathogen perception and host gene
530 regulation. In *Plant Signaling and Behavior* (Vol. 8, Issue 3).
531 <https://doi.org/10.4161/psb.23468>
- 532 Porter, K., Shimono, M., Tian, M., & Day, B. (2012). Arabidopsis Actin-Depolymerizing
533 Factor-4 Links Pathogen Perception, Defense Activation and Transcription to
534 Cytoskeletal Dynamics. *PLoS Pathogens*, 8(11).
535 <https://doi.org/10.1371/journal.ppat.1003006>
- 536 Raffaele, S., Bayer, E., Lafarge, D., Cluzet, S., Retana, S. G., Boubekur, T., Castel, N. L.,
537 Carde, J. P., Lherminier, J., Noiro, E., Jeunemaître, B. S., Traineau, J. L., Moreau, P., Ott,
538 T., Maule, A. J., Reymond, P., Simon-Plas, F., Farmer, E. E., Bessoule, J. J., & Mongrand,
539 S. (2009). Remorin, a solanaceae protein resident in membrane rafts and
540 plasmodesmata, impairs potato virus X movement. *The Plant Cell*, 21(5), 1541–1555.
541 <https://doi.org/10.1105/TPC.108.064279>
- 542 Raffaele, S., Mongrand, S., Gamas, P., Niebel, A., & Ott, T. (2007). Genome-wide annotation
543 of remorins, a plant-specific protein family: Evolutionary and functional perspectives.
544 *Plant Physiology*, 145(3), 593–600. <https://doi.org/10.1104/pp.107.108639>
- 545 Ressad, F., Didry, D., Xia, G. X., Hong, Y., Chua, N. H., Pantaloni, D., & Carlier, M. F. (1998).
546 Kinetic analysis of the interaction of actin-depolymerizing factor (ADF)/cofilin with G-
547 and F-actins: Comparison of plant and human ADFs and effect of phosphorylation.
548 *Journal of Biological Chemistry*, 273(33), 20894–20902.
549 <https://doi.org/10.1074/jbc.273.33.20894>
- 550 Rocher, M., Simon, V., Jolivet, M. D., Sofer, L., Deroubaix, A. F., Germain, V., Mongrand, S., &
551 German-Retana, S. (2022). StREM1.3 REMORIN Protein Plays an Agonistic Role in
552 Potyvirus Cell-to-Cell Movement in *N. benthamiana*. *Viruses*, 14(3).
553 <https://doi.org/10.3390/V14030574>
- 554 Schanda, P., & Brutscher, B. (2005). Very fast two-dimensional NMR spectroscopy for real-
555 time investigation of dynamic events in proteins on the time scale of seconds. *Journal*
556 *of the American Chemical Society*, 127(22), 8014–8015.
557 https://doi.org/10.1021/JA051306E/SUPPL_FILE/JA051306ESI20050412_060033.PDF
- 558 Schindelin, J., Arganda-Carreras, I., Frise, E., Kaynig, V., Longair, M., Pietzsch, T., Preibisch, S.,
559 Rueden, C., Saalfeld, S., Schmid, B., Tinevez, J. Y., White, D. J., Hartenstein, V., Eliceiri,
560 K., Tomancak, P., & Cardona, A. (2012). Fiji: an open-source platform for biological-
561 image analysis. *Nature Methods* 2012 9:7, 9(7), 676–682.
562 <https://doi.org/10.1038/nmeth.2019>
- 563 Sezgin, E., Levental, I., Mayor, S., & Eggeling, C. (2017). The mystery of membrane

564 organization: composition, regulation and roles of lipid rafts. *Nature Reviews*.
565 *Molecular Cell Biology*, 18(6), 361–374. <https://doi.org/10.1038/NRM.2017.16>
566 Smokvariska, M., Francis, C., Platre, M. P., Fiche, J. B., Alcon, C., Dumont, X., Nacry, P., Bayle,
567 V., Nollmann, M., Maurel, C., Jaillais, Y., & Martiniere, A. (2020). A Plasma Membrane
568 Nanodomain Ensures Signal Specificity during Osmotic Signaling in Plants. *Current*
569 *Biology*, 30(23), 4654–4664.e4. <https://doi.org/10.1016/j.cub.2020.09.013>
570 Su, C., Rodriguez-Franco, M., Lacey, B., Nebel, N., Hernandez-Reyes, C., Liang, P., Schulze, E.,
571 Mymrikov, E. V., Gross, N. M., Knerr, J., Wang, H., Siukstaite, L., Keller, J., Libourel, C.,
572 Fischer, A. A. M., Gabor, K. E., Mark, E., Popp, C., Hunte, C., ... Ott, T. (2023).
573 Stabilization of membrane topologies by proteinaceous remorin scaffolds. *Nature*
574 *Communications* 2023 14:1, 14(1), 1–16. <https://doi.org/10.1038/s41467-023-35976-5>
575 Szymanski, W. G., Zauber, H., Erban, A., Gorka, M., Wu, X. N., & Schulze, W. X. (2015).
576 Cytoskeletal Components Define Protein Location to Membrane Microdomains.
577 *Molecular & Cellular Proteomics : MCP*, 14(9), 2493–2509.
578 <https://doi.org/10.1074/MCP.M114.046904>
579 Tian, M., Chaudhry, F., Ruzicka, D. R., Meagher, R. B., Staiger, C. J., & Day, B. (2009).
580 Arabidopsis actin-depolymerizing factor AtADF4 mediates defense signal transduction
581 triggered by the pseudomonas syringae effector AvrPphB 1[w][OA]. *Plant Physiology*,
582 150(2), 815–824. <https://doi.org/10.1104/pp.109.137604>
583 Troshin, P. V., Procter, J. B., & Barton, G. J. (2011). Java bioinformatics analysis web services
584 for multiple sequence alignment—JABAWS:MSA. *Bioinformatics*, 27(14), 2001–2002.
585 <https://doi.org/10.1093/BIOINFORMATICS/BTR304>
586 Üstün, S., Hafrén, A., Liu, Q., Marshall, R. S., Minina, E. A., Bozhkov, P. V., Vierstra, R. D., &
587 Hofius, D. (2018). Bacteria Exploit Autophagy for Proteasome Degradation and
588 Enhanced Virulence in Plants. *The Plant Cell*, 30(3), 668–685.
589 <https://doi.org/10.1105/TPC.17.00815>
590 Wang, M. S., & Huse, M. (2022). Phollow the phosphoinositol: Actin dynamics at the B cell
591 immune synapse. *The Journal of Cell Biology*, 221(9).
592 <https://doi.org/10.1083/JCB.202208015>
593 Wright, P. E., & Dyson, H. J. (2014). Intrinsically disordered proteins in cellular signalling and
594 regulation. *Nature Reviews Molecular Cell Biology* 2015 16:1, 16(1), 18–29.
595 <https://doi.org/10.1038/nrm3920>
596 Yang, M., Zhang, Y., Xie, X., Yue, N., Li, J., Wang, X. B., Han, C., Yu, J., Liu, Y., & Li, D. (2018).
597 Barley stripe mosaic virus γ B Protein Subverts Autophagy to Promote Viral Infection by
598 Disrupting the ATG7-ATG8 Interaction. *The Plant Cell*, 30(7), 1582–1595.
599 <https://doi.org/10.1105/TPC.18.00122>
600
601

602 **FIGURE LEGENDS**

603 **Figure 1 | Phosphorylation modulates StREM1.3 intrinsically disordered domain.**

604 **A.** Representative confocal micrograph showing the surface of *N. benthamiana* leaf epidermal
605 cells expressing YFP-StREM1.3^{WT} and YFP-StREM1.3^{DDD} (left) and corresponding quantification
606 of YFP-StREM1.3^{WT} and YFP-StREM1.3^{DDD} spatial clustering index (right). Graphs are notched
607 box plots, scattered data points show measurements, colors indicate independent
608 experiments, n=38 cells for YFP-StREM1.3 and n=39 cells for YFP-StREM1.3^{DDD}. P values report
609 two-tailed non-parametric Mann-Whitney test. Scale bar indicates 5 μ m.

610 **B.** ¹H-¹⁵N HMQC spectra of StREM¹⁻¹¹⁶ before (black) and after (blue) addition of AtCPK3. Peaks
611 labelled 1,2 and 3 appeared over time. Each spectrum was acquired using 2 scans for an
612 experimental time of 1 min 42 s each. Temperature: 20°C.

613 **C.** NMR intensities of peaks 1, 2 and 3 (Figure 1B) over time after the addition of AtCPK3.

614

615 **Figure 2 | Comparative analysis of StREM1.3 and StREM1.3^{DDD} interactomes in SUY2H.**

616 **A-B.** Drop-tests of SUY2H assays performed with yeast clones retrieved from two independent
617 side-by-side screens performed using Cub-StREM1.3 (**A**) or Cub-StREM1.3^{DDD} (**B**) as bait and
618 constructs from the *N. benthamiana* leaf epidermis cDNA library.

619 **C.** Quantification of the number of positive clones retrieved from Cub-StREM1.3 and Cub-
620 StREM1.3^{DDD} screens, observed on -AHLW plates 4 days after transformations normalized by
621 transformation efficiency for each screen (expressed in ‰ of theoretically tested clones).
622 Data points show values obtained for individual -AHLW plates. P values report two-tailed non-
623 parametric Mann-Whitney test.

624 **D.** Venn diagram depicting the number of proteins identified with Cub-StREM1.3 and Cub-
625 StREM1.3^{DDD}.

626

627 **Figure 3 | Functional analysis of StREM1.3's putative interactors upon PVX infection.**

628 **A.** Representative images of PVX:GFP infection foci of *N. benthamiana* leaves expressing
629 empty vector (control condition) and 2 selected HA-tagged candidates. Scale bar = 500 μ m.

630 **B.** Quantification of PVX infection assays. The table is color coded based on the mean PVX:GFP
631 infection foci area observed upon the overexpression of individual candidates normalized to
632 the mean PVX:GFP infection foci area of the corresponding empty vector condition. Each
633 candidate was N-terminally-fused to an HA-tag and expressed under the control of a 35S

634 promoter. Number of infection foci n=182 for HA-NbMT2B, n=219 for HA-NbPIP1;3, n=177
635 for HA-NbCRT3, n=249 for HA-NbTRX4, n=208 for HA-NbDRM1, n=223 for HA-NbGST8, n=114
636 for HA-ATG8i, n=228 for HA-TIP2;1, n=209 for HA-NbADF3, n=175 for HA-RabA4A. Stars report
637 by Dunn's comparisons test, p<0.05: * p<0.01: **, p<0.001: ***, non-significant (n.s): p>0.05.

638

639 **Figure 4 | StADF2 limits PVX cell-to-cell movement in a REMORIN-dependent manner.**

640 **A.** Immunoprecipitation of GFP-StREM1.3 transiently co-expressed with either RFP or RFP-
641 StADF2 in *N. benthamiana*. Blot stained with Ponceau is presented to show loading. Western
642 blots were probed with α -GFP or α -RFP antibodies.

643 **B-C.** PVX infection assays. Representative micrograph of PVX:GFP infection foci upon
644 expression of RFP-StADF2 in WT and stable *REMORINs* knock-down transgenic *N.*
645 *benthamiana* independent lines #1.4 and #10.2 (**B**) and corresponding quantification (**C**).
646 PVX:GFP foci are normalized based on the average area observed in the absence of RFP-
647 StADF2 overexpression for each genotype. Graphs are notched box plots, scattered data
648 points show measurements, colors indicate independent experiments, number of infections
649 foci n=114 for WT, n=113 for #1.4 and n=104 for #10.2. Conditions which do not share a letter
650 are significantly different in Holm-Bonferroni's multiple comparison test (p< 0.0001). Scale
651 bar indicates 500 μ m.

652

653 **Figure 5 | StADF2 alters StREM1.3 nanodomains to inhibit PVX cell-to-cell movement.**

654 **A-B.** Plasma membrane organization of YFP-StREM1.3 with or without co-expression of HA-
655 StADF2 and HA-StADF2^{S6D}. Representative confocal micrograph (**A**) and corresponding
656 quantification of YFP-StREM1.3 spatial clustering index (**B**). Graphs are notched box plots,
657 scattered data points show measurements, colors indicate independent experiments, n=38
658 cells for YFP-StREM1.3, n=38 cells for YFP-StREM1.3 + HA-StADF2 and n=38 cells for YFP-
659 StREM1.3 + HA-StADF2^{S6D}. Conditions which do not share a letter are significantly different in
660 Holm-Bonferroni's multiple comparison test (p< 0.0001). Scale bar indicates 2 μ m.

661 **C-D.** PVX infection assays. Representative micrograph of PVX:GFP infection foci upon
662 expression of HA-StADF2 or HA-StADF2^{S6D} (**C**) and corresponding quantification (**D**). Graphs
663 are notched box plots, scattered data points show measurements, colors indicate
664 independent experiments, number of infections foci n=39 for mock, n=38 foci for HA-StADF2

665 and n=31 foci for HA-StADF2^{S6D}. Conditions which do not share a letter are significantly
666 different in Dunn's multiple comparison test ($p < 0.0001$). Scale bar indicates 500 μm .

667

668

669 **Figure supplemental 1 | StREM1.3 N-terminal domain is intrinsically disordered.**

670 **A.** SDS-PAGE of purified untagged StREM1.3¹⁻¹¹⁶ under native and denaturing conditions.

671 **B.** ¹H-¹⁵N HMQC spectra of REM¹⁻¹¹⁶ purified under native (black) or denaturing conditions
672 using 7M of urea (red). Temperature: 10°C.

673

674 **Figure supplemental 2 | AtCPK3 phosphorylates StREM1.3¹⁻¹¹⁶ under NMR conditions.**

675 **B.** *In vitro* kinase assay to confirm phosphorylation of StREM1.3¹⁻¹¹⁶ under liquid-state NMR
676 conditions. StREM1.3¹⁻¹¹⁶ incubated for either 30 min or 2 h with wild-type AtCPK3-GST
677 untreated (WT) or heat-inactivated (D).

678

679 **Figure supplemental 3 | Cub-StREM1.3 and Cub-StREM1.3^{DDD} are functional baits in SUY2H.**

680 **A-B.** Drop-tests of SUY2H assays testing binary interactions between Cub-StREM1.3 (**A**) with
681 NubG-StREM1.3 or StREM1.3-NubG, or Cub-StREM1.3^{DDD} (**B**) with NubG-StREM1.3 or
682 StREM1.3-NubG.

683 **C.** Representative micrograph of GFP-StREM1.3 and GFP-StREM1.3^{DDD} imaged in proliferating
684 *S. cerevisiae*. Scale bar indicates 2 μm .

685

686 **Figure supplemental 4 | Rational design of the SUY2H screens.**

687 **A.** Schematics depicting the experimental design. Cub-StREM1.3 and Cub-StREM1.3^{DDD} were
688 used as baits against a cDNA library obtained from PVX-infected *N. benthamiana* epidermis
689 in side-by-side screens.

690 **B.** Picture of a *N. benthamiana* leaf peeled. Scale bar indicates 5 cm.

691 **C.** Confocal micrograph of peeled *N. benthamiana* epidermis infected with PVX:GFP. Scale bar
692 indicates 5 μm .

693

694 **Figure supplemental 5 | Western blots analyses of the expression of protein candidates in**
695 **PVX cell-to-cell movement assays.**

696 Protein extracts from *N. benthamiana* leaves expressing HA-tagged candidates were analyzed
697 by western blots with α -HA antibody. In case of multiple bands, a white star points out the
698 band corresponding to the expected molecular weight. Abbreviations are as followed:
699 Dormancy-associated Protein-like 1 (NbDRM1), Calreticulin 3 (NbCRT3), Glutathione S-
700 transferase 8 (NbGST8), Plasma membrane intrinsic protein 1C (NbPIP1C), Actin
701 Depolymerizing Factor 3 (NbADF3), Metallothionein 2B (NbMT2B), Delta tonoplast integral
702 protein (NbTIP2;1), Thioredoxin superfamily protein 4 (NbTRX4), Autophagy 8I (NbATG8i),
703 GTPase protein (NbRabA4A).

704

705 **Figure supplemental 6 | StADF2 affects YFP-StREM1.3 nanodomain organization and YFP-**
706 **StREM1.3 nanodomain relies on the actin cytoskeleton integrity.**

707 **A-B.** Plasma membrane organization of YFP-StREM1.3 with or without co-expression of RFP-
708 StADF2. Representative confocal micrograph (**A**) and corresponding quantification of YFP-
709 StREM1.3 spatial clustering index (**B**) are shown. Graphs are notched box plots, scattered data
710 points show measurements, colors indicate independent experiments, n=39 cells for YFP-
711 StREM1.3, n=41 cells for YFP-StREM1.3 + RFP-StADF2. P values report two-tailed non-
712 parametric Mann-Whitney test. Scale bar indicates 5 μ m.

713 **C-D.** Plasma membrane organization of YFP-StREM1.3 co-expressed with LifeAct-mCherry to
714 label actin upon 80 μ M Cytochalasin D treatment for 24h or corresponding mock control
715 (DMSO). Representative confocal micrograph (**C**) and corresponding quantification of YFP-
716 StREM1.3 spatial clustering index (**D**) are shown. Graphs are notched box plots, scattered data
717 points show measurements, colors indicate independent experiments, n=34 cells for mock
718 treatment, n=34 cells for Cytochalasin D treatment. P values report two-tailed non-parametric
719 Mann-Whitney test. Scale bar indicates 5 μ m.

720

721 **Figure supplemental 7 | Serine 6 is conserved among ADFs.**

722 Sequence logo of ADFs N-termini generated from 459 protein sequences retrieved from 101
723 plant species using BLASTp and StADF2 as query.

724

725

726 MATERIALS AND METHODS

727 Plant materials, culture and transformation

728 *N. benthamiana* plants were cultivated in controlled conditions (16 h photoperiod, 25 °C). *N.*
729 *benthamiana* plants were transiently transformed using the *Agrobacterium tumefaciens*
730 strain GV3101 as previously described (Gronnier et al., 2017). For subcellular localization
731 study and western blotting analyses, plants were analyzed 2 days after infiltration (dai). For
732 PVX:GFP spreading assays, plants were observed 5 dai. The *N. benthamiana* transgenic RNAi
733 knock-down lines hpREM #1.4 and hpREM #10.2 were previously described (Perraki et al.,
734 2018).

735

736 PVX cell-to-cell movement

737 The assays were conducted as previously described (Perraki et al., 2018). *Agrobacteria*
738 solution ($OD^{600nm} = 0.001$) carrying PVX:GFP and the helper plasmid pSoup was mixed to equal
739 volume with *agrobacteria* carrying a binary plasmid encoding for tested proteins ($OD^{600nm} =$
740 0.2) and co-infiltrated in leaves of 3 weeks old *N. benthamiana*. Plants were observed at 5 dai
741 using Zeiss Axiozoom V16 equipped with a UV lamp, an excitation filter (450-490 nm) and an
742 emission filter (500-550 nm) to detect GFP signal. Foci were automatically analyzed using the
743 Fiji software (Schindelin et al., 2012) via a homemade macro.

744

745 Membrane-based split-ubiquitin Yeast two-hybrid

746 Split ubiquitin assays were performed using the yeast two-hybrid system from DUAL
747 membrane system (Dual systems Biotech AG). StREM1.3^{WT} and StREM1.3^{S74D T86D S91D} coding
748 sequences were amplified by PCR using Sfil restriction site-containing primers (Supplemental
749 Table 2) and subsequently cloned in pBT3N bait and pPR3N prey plasmids. To test the
750 functionality of StREM1.3 in this system, THY.AP4 cells were sequentially transformed with
751 pBT3N:StREM1.3 and pPR3N:StREM1.3 or pPR3N empty vector as a negative control. The
752 cDNA library was constructed following the manufacturer's instructions (Evrogen) using
753 approximately 700 ng total RNA of epidermis peeled from healthy and PVX-infected *N.*
754 *benthamiana* leaves, harvested three days after agroinfiltration. For screening, NubG-cDNA
755 library was used for transformation of THY.AP4 yeast strain *MATa*, *ura3-*, *leu2-*, *lexA-*
756 *lacZ::TRP1*, *lexA::HIS3*, *lexA::ADE2*) previously transformed with pBT3N:StREM1.3 or
757 pBT3N:StREM1.3^{DDD}. Positive clones were selected on synthetic medium (SD) lacking adenine,

758 histidine, tryptophan and leucine (-AHLW) and subsequently tested for β -galactosidase
759 activity. To measure β -galactosidase activity, yeasts were grown on SD-TL for two days at
760 28°C. Plates were then covered with a X-Gal-agarose buffer (0.5% agarose, 0.5 M phosphate
761 buffer, pH 7.0, 0.002% X-Gal) and incubated at 37°C for 10 to 20 min. To identify the proteins
762 expressed in Yeast positive clones obtained from the SUY2H exploratory screens, the
763 corresponding plasmids were isolated from Yeast, subsequently propagated in *E. coli*, isolated
764 and analyzed by Sanger sequencing. Individual coding sequences were BLAST against *N.*
765 *benthamiana* Genome v1.0.1 predicted cDNA (<https://solgenomics.net/>).

766

767 ***In silico* analyses**

768 During SUY2H exploratory screens, identification of proteins expressed in yeast positive
769 clones was retrieved using BLASTn algorithm against *N. benthamiana* Genome v1.0.1
770 predicted cDNA. Closest orthologs of the identified StREM1.3-interacting proteins in *A.*
771 *thaliana* were retrieved on The Arabidopsis Information Resource TAIR using BLASTp
772 algorithm. The 500 hundreds closest homologs of StADF2 were retrieved from 101 plant
773 species in Phytozome (Goodstein et al., 2012) using BLASTp. Protein alignment was computed
774 using MULTiple Sequence Comparison by Log-Expectation (MUSCLE; (Edgar, 2004)) using
775 BLOSUM62 matrix, an -sv profile scoring method with following parameters: Anchor
776 spacing:32, diagonal break:1, diagonal length:24, diagonal margin:5, gap extension penalty:-
777 1, gap open penalty:-12, hydro:5 and hydro factor1.2, through the JABAWS server (Troshin et
778 al., 2011). Among 500 ADF protein sequences, 41 are predicted splice variants lacking the first
779 7 amino acids and were excluded for sequence logo analysis, generated using WebLogo
780 (Crooks et al., 2004).

781

782 **Molecular cloning**

783 Candidate genes selected from the screen were cloned from the cDNA bank generated for
784 the SUY2H screen using primers designed to amplify full length coding sequences. All vector
785 constructs were generated using classical Gateway cloning strategies
786 (www.lifetechnologies.com), using pDONR211 and pDONR207 as entry vectors and
787 pK7WGY2, pK7YWG2, pK7WGR2, pK7RWG2 (Karimi et al., 2002), pGWB14, pGWB15
788 (Nakagawa et al., 2007) and pSite BiFC as destination vectors (Martin et al., 2009). StADF2
789 and StADF2^{S6D} bearing attL sequences were synthesized (<https://www.genscript.com/>) in a

790 pUC57 vector to be cloned in aforementioned destination vectors. The StREM1.3^{S74D T86D S91D}
791 was previously described (Perraki et al., 2018). For GFP-StREM1.3 expression in
792 *Saccharomyces cerevisiae*, StREM1.3^{WT} and StREM1.3^{DDD} coding sequences were PCR
793 amplified with oligonucleotides listed in supplemental table S2, digested by BamHI–NsiI and
794 cloned at BamHI–PstI sites of the plasmids p2717 (pCM189 modified by the introduction of a
795 myc epitope tag downstream of the tet promoter (Escusa et al., 2006)). The resulting plasmids
796 (respectively pMC101 and pMC104) were transformed into a wild type strain BY4741 (*MAT α* ,
797 *his3 Δ 1*, *leu2 Δ 0*, *met15 Δ 0*, *ura3 Δ 0*). All plasmids were propagated using the NEB10 *E. coli*
798 strain (New England Biolabs).

799

800 **Protein expression in *E. coli* and purification**

801 StREM1.3¹⁻¹¹⁶ was obtained as previously described (Legrand et al., 2022). Shortly, StREM1.3¹⁻
802 ¹¹⁶ was expressed in BL21-DE3 cells in minimal medium with ¹³C-labelled glucose and ¹⁵NH⁴Cl,
803 by addition of 1 mM IPTG at OD⁶⁰⁰ = 0.6-0.8 and incubation at 37°C for 3h. Cells were lysed by
804 sonication and the supernatant was loaded onto a HisTrap column (GE Healthcare)
805 equilibrated in 20 mM HEPES 150 mM NaCl, 20 mM imidazole, 0.02% NaN₃, pH=7.4 and eluted
806 with 20 mM HEPES, 150 mM NaCl, 500 mM imidazole, 0.02% NaN₃, pH=7.4. For TEV cleavage,
807 eluted StREM1.3¹⁻¹¹⁶ was adjusted to 1 mM DTT and 0.5 mM EDTA, the TEV protease was
808 added in a ~1/200 TEV/REM¹⁻¹¹⁶ mass ratio and the reaction was incubated for 3h at room
809 temperature then desalted against 10 mM HEPES, 50 mM NaCl, 0.02% NaN₃, pH=7.5 with a
810 HiPrep column (GE Healthcare). Under native conditions, StREM1.3¹⁻¹¹⁶ was loaded onto a
811 HisTrap column equilibrated with 20 mM HEPES, 150 mM NaCl, 0.02% NaN₃, pH=7.4 and
812 eluted with the same elution buffer as above. Under denaturing conditions, this step was
813 performed in buffers containing 7M urea. Finally, StREM1.3¹⁻¹¹⁶ was desalted again against 10
814 mM HEPES, 50 mM NaCl 0.02%, NaN₃ pH=7.5. AtCPK3-GST recombinant protein was
815 produced in BL21-DE3-pLys and purified as previously reported (Legrand, et al., 2022). As a
816 negative control, AtCPK3-GST was inactivated by heating at 95°C for 10 min.

817

818 ***In vitro* phosphorylation**

819 *In vitro* phosphorylation of 0.5 mM of StREM1.3¹⁻¹¹⁶ by AtCPK3 was done as previously
820 published (Legrand et al., 2022). For NMR analysis, the StREM1.3¹⁻¹¹⁶ sample was adjusted to

821 10 mM MgCl₂, 1 mM CaCl₂, 1 mM DTT and 3 mM ATP. The reaction was initiated by the
822 addition of 88 μM of AtCPK3 and incubation at 20°C.

823

824 **Liquid-state Nuclear magnetic resonance (NMR) spectroscopy**

825 NMR spectroscopy was performed on a Bruker Advance NEO spectrometer operating at 700
826 MHz for proton with a TXI 5 mm probe. The samples were adjusted to 9/1 H₂O/D₂O (v/v) to
827 lock the magnetic field. Monitoring of phosphorylation kinetics was performed using a ¹H-¹⁵N
828 HMQC pulse sequence (Schanda & Brutscher, 2005), with 2 scans per timepoint (*i.e* 1 min 42
829 s to acquire one spectrum). The spectra were processed and analyzed using TopSpin (Bruker).

830

831 **Confocal laser scanning microscopy and image analysis**

832 Live imaging was performed using a Zeiss LSM 880 confocal laser scanning microscopy system
833 using a 68x objective and the AiryScan detector. YFP fluorescence was observed using an
834 excitation wavelength of 488 nm and an emission wavelength of 453nm. RFP and mCherry
835 fluorescence were observed using an excitation wavelength of 561 nm and detected at 579
836 nm. Acquisition parameters were kept identical across experiments. The SCI was calculated
837 as previously described (Gronnier et al., 2017). Briefly, 10 μm lines were plotted across the
838 samples and the SCI was calculated by dividing the mean of the 5 % highest values by the
839 mean of 5 % lowest values. Three lines were randomly plotted per cell.

840 To disrupt actin cytoskeleton integrity, Cytochalasin D (40 μg/mL) dissolved in DMSO was
841 infiltrated 24 hours before observation, infiltration of DMSO for 24 hours was used as
842 corresponding mock control.

843 Yeast cells were observed on a fully-automated Zeiss 200M inverted microscope (Carl Zeiss,
844 Thornwood, NY, USA) equipped with an MS-2000 stage (Applied Scientific Instrumentation,
845 Eugene, OR, USA), a Lambda LS 300-Watt xenon light source (Sutter, Novato, CA, USA), and a
846 100 × 1.4 NA Plan-Apochromat objective. GFP imaging was done using a FITC filter (excitation,
847 HQ487/25; emission, HQ535/40; beam splitter, Q505lp). Images were acquired using a Prime
848 sCMOS 95B camera (Photometrics, Tucson, AZ, USA). The microscope, camera, and shutters
849 (Uniblitz, Rochester, NY, USA) were controlled by SlideBook software 5. 0. (Intelligent Imaging
850 Innovations, Denver, CO, USA).

851

852 **Western-blotting**

853 Proteins were extracted from *N. benthamiana* leaf tissue transiently expressing HA-tagged
854 proteins in 100 mM Tris (pH 7.5) containing 3% SDS, 5mM EDTA and 2% Protease inhibitor
855 (Roche, Complete) boiled for 10 min at 70°C in SDS loading buffer, and cleared by
856 centrifugation. The protein extracts were then separated by SDS-PAGE, transferred to
857 polyvinylidene difluoride (PVDF) membranes (BioRad), blocked with 5% skimmed milk in TBS-
858 Tween 0.05%, and incubated with an anti-HA antibody coupled to horse radish peroxidase
859 (Roche). The resulting western-blotting were developed using an ECL Prime Kit (GE Healthcare)
860 and detected with an ImageQuant 800 (Amersham).

861

862 **Co-immunoprecipitation**

863 Immunoprecipitation assays were performed as previously described in (Dagdaz et al., 2016)
864 with minor modifications. Approximately 3 g of *N. benthamiana* leaves were ground with a
865 mortar and pestle in liquid nitrogen and homogenized in 6 mL of extraction buffer (50 mM
866 Tris- HCl, pH 7.5, 150 mM NaCl, 10% glycerol, 5 mM DTT, 1 mM EDTA, 2% (w/v)
867 polyvinylpyrrolidone, 1% (v/v) CComplete protease inhibitor cocktail [Roche], 0.1% (v/v)
868 IGEPAL). Samples were then centrifuged for 20 min with 2000 x g at 4°C. Immunoprecipitation
869 was performed by adding 30 µl of GFP-Trap coupled to agarose beads (ChromoTek) and
870 samples were continuously agitated for 2 hours at 4°C. Beads were subsequently washed five
871 times with extraction buffer and eluted with 30 µl of 2X Laemmli buffer at 70 °C for 10
872 minutes.

873

874 **Statistical analyses**

875 Statistical analyses were carried out using Prism 6.0 software (GraphPad). As mentioned in
876 the figure legends, statistical significances were assessed using non-parametric Kruskal-Wallis
877 bilateral tests combined with post-hoc Dunn's multiple pairwise comparisons, or using a two-
878 way non-parametric Mann-Whitney test.

879

880 **Accession numbers**

881 NbADF3 (NbS00025994g0001.1), NbCRT3 (NbS00018258g0010.1), NbMT2B
882 (NbC25904295g0003.1), NbATG8I (NbS00005942g0011.1), NbPIP1C (NbS00006841g0003.1),
883 NbTIP2;1, (NbS00006781g0007.1), NbDRM1 (NbS00004204g0005.1), NbGST8

884 (NbS00007668g0012.1), NbTRXH4 (NbS00049748g0003.1), NbRabA4A
885 (NbS00057294g0003.1), StREM1.3 (NP_001274989), StADF2 (Soltu.DM.04G007350).

886

887 **ACKNOWLEDGEMENTS**

888 We thank the Bordeaux Imaging Center, part of the National Infrastructure France-BioImaging
889 supported by the French National Research Agency (ANR-10-INBS-04). This work was
890 supported by the French National Research Agency (grant no. ANR-19-CE13-0021 to SGR, SM,
891 VG and doctoral fellowships to MDJ, PG and JG), and the German Research Foundation (DFG)
892 grant CRC1101-A09 to JG, the IPS2 benefits from the support of the LabEx Saclay Plant
893 Sciences-SPS (ANR- 10-LABX-0040-SPS). We thank Isabel Monte and members of the
894 NanoSignaling Lab for discussions and critical reading of the manuscript.

895

896 The authors declare no conflict of interest

897

898 **AUTHORS CONTRIBUTION**

899 ALe purified labelled StREM1.3¹⁻¹¹⁶ and performed NMR experiments

900 ALe, BH and AL analyzed NMR results

901 JG and VG built the cDNA libraries

902 AML and IS localized fluorescent tagged StREM1.3 in yeast

903 JG performed the split-ubiquitin assays

904 PG, MDJ and JG performed and analyzed virus propagation

905 MDJ performed confocal microscopy

906 MB performed in vitro kinase assay

907 JG, MD, BH, AL, VG, SM designed the project

908 MDJ and JG assembled the figures

909 MDJ and JG wrote the manuscript with input from all authors.

bioRxiv preprint doi: <https://doi.org/10.1101/2023.01.25.525625>; this version posted January 26, 2023. The copyright holder for this preprint (which was not certified by peer review) is the author/funder, who has granted bioRxiv a license to display the preprint in perpetuity. It is made available under aCC-BY 4.0 International license.

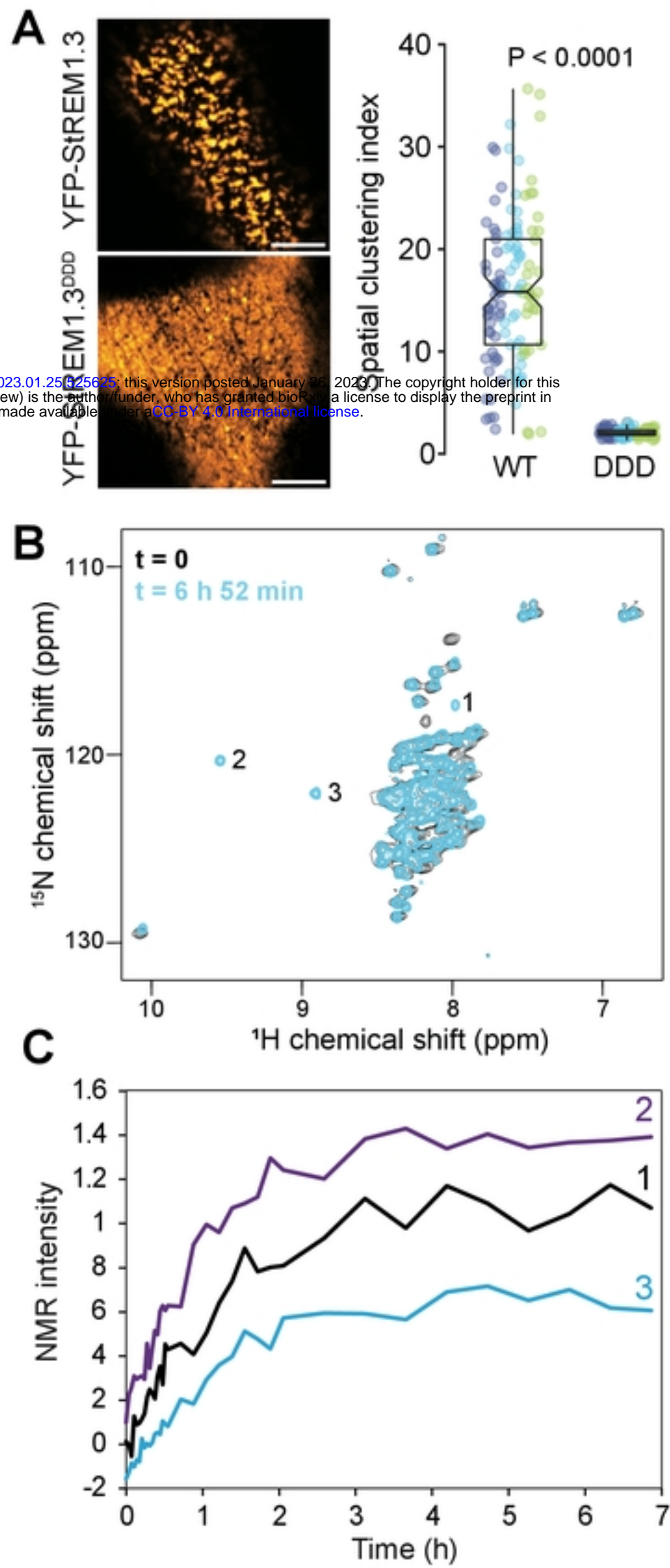


Figure 1 | Phosphorylation modulates StREM1.3 intrinsically disordered domain.

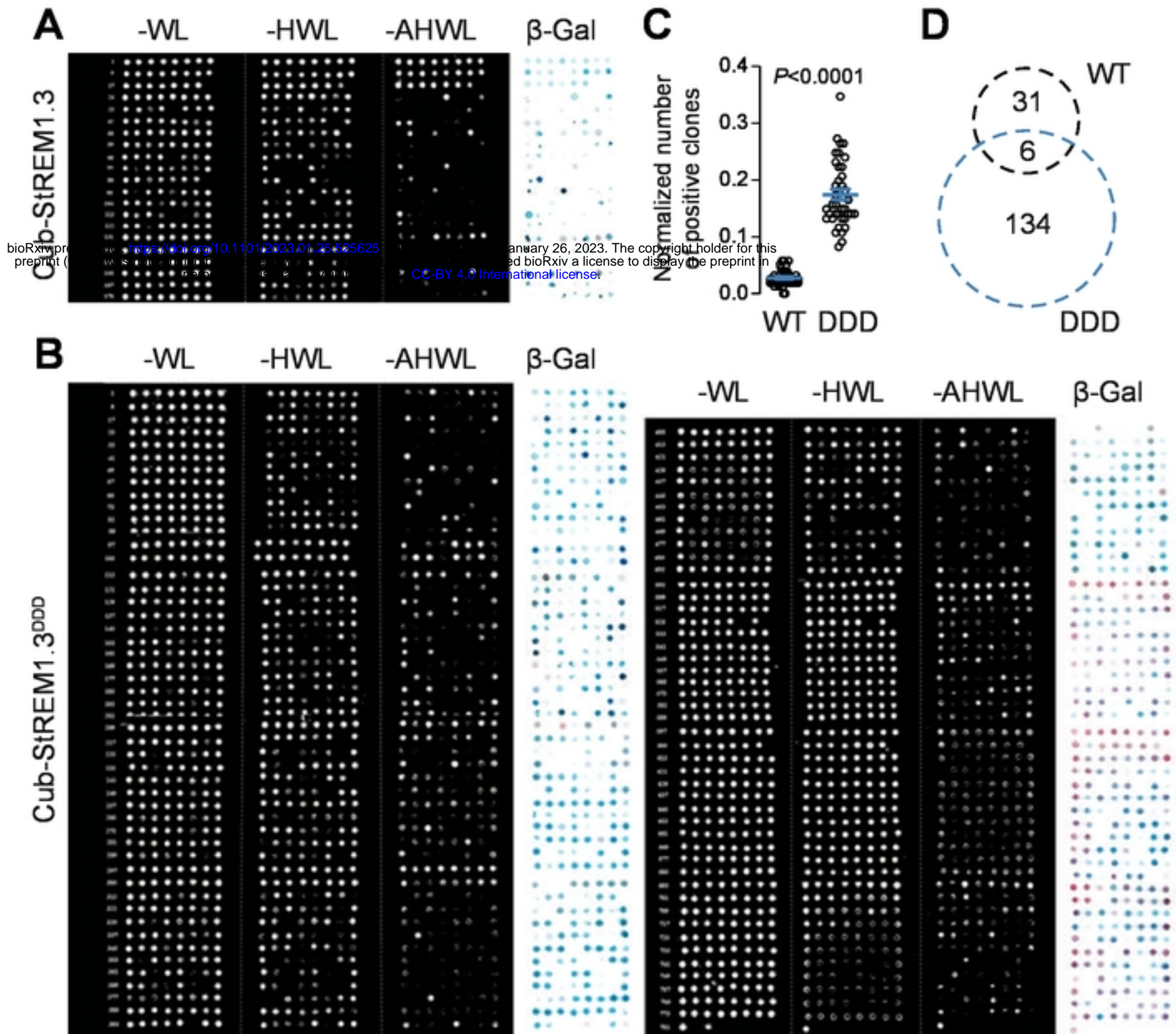


Figure 2 | Comparative analysis of StREM1.3 and StREM1.3^{DDD} interactomes in SUY2H.

bioRxiv preprint doi: <https://doi.org/10.1101/2023.01.25.525625>; this version posted February 26, 2023. The copyright holder for this preprint (which was not certified by peer review) is the author/funder, who has granted bioRxiv a license to display the preprint in perpetuity. It is made available under aCC-BY 4.0 International license.

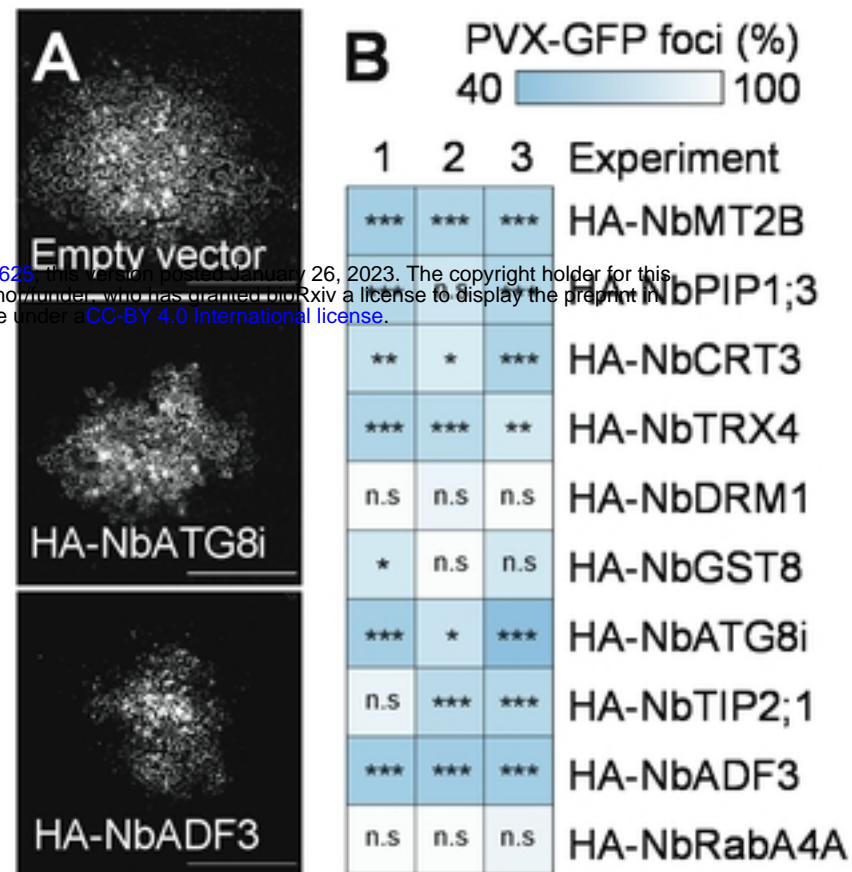


Figure 3 | Functional analysis of StREM1.3's putative interactors upon PVX infection.

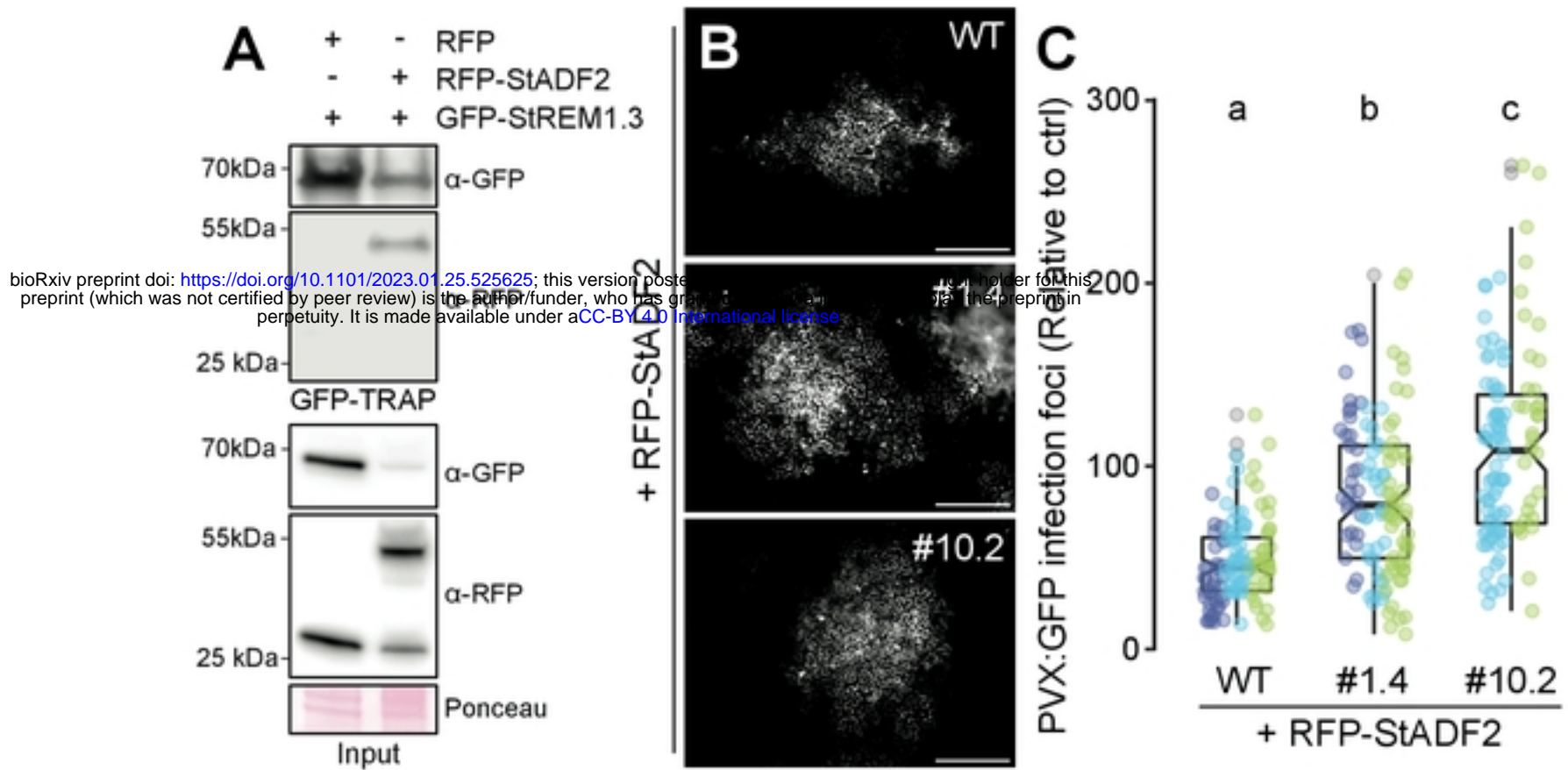


Figure 4 | StADF2 limits PVX cell-to-cell movement in a REMORIN-dependent manner.

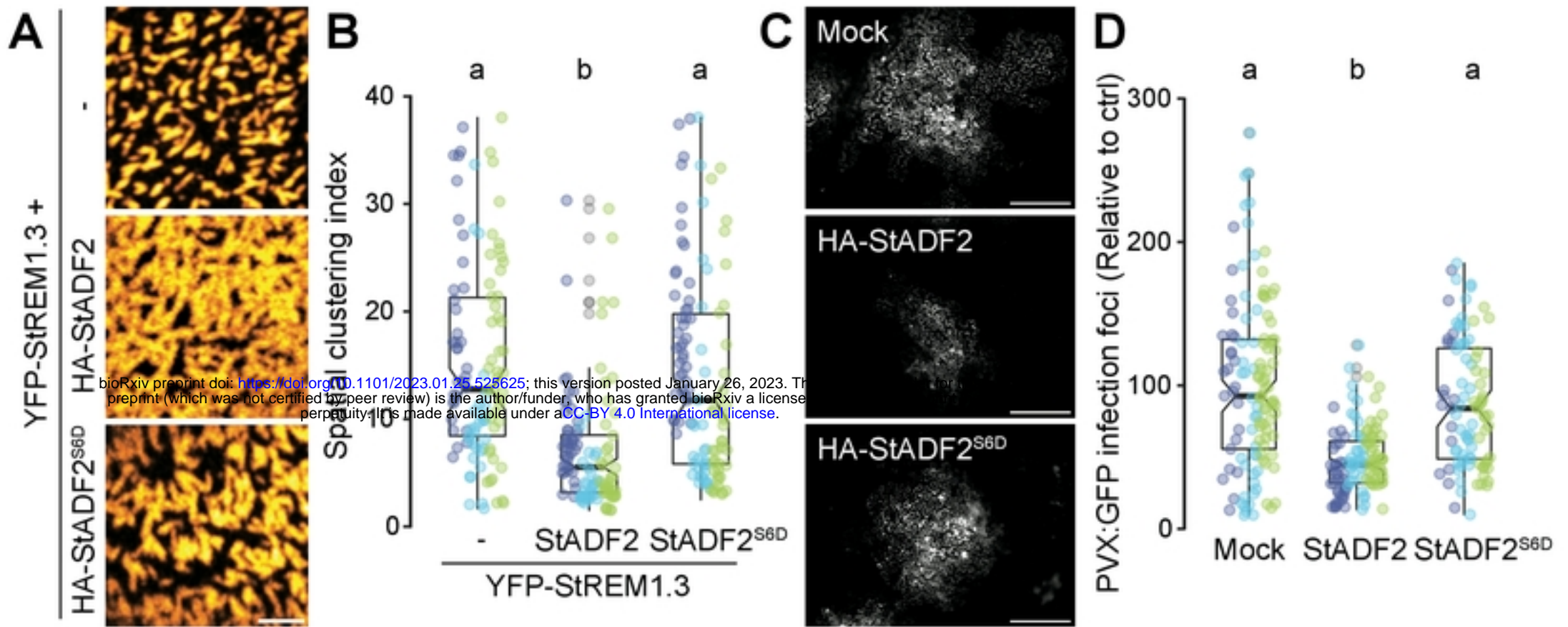
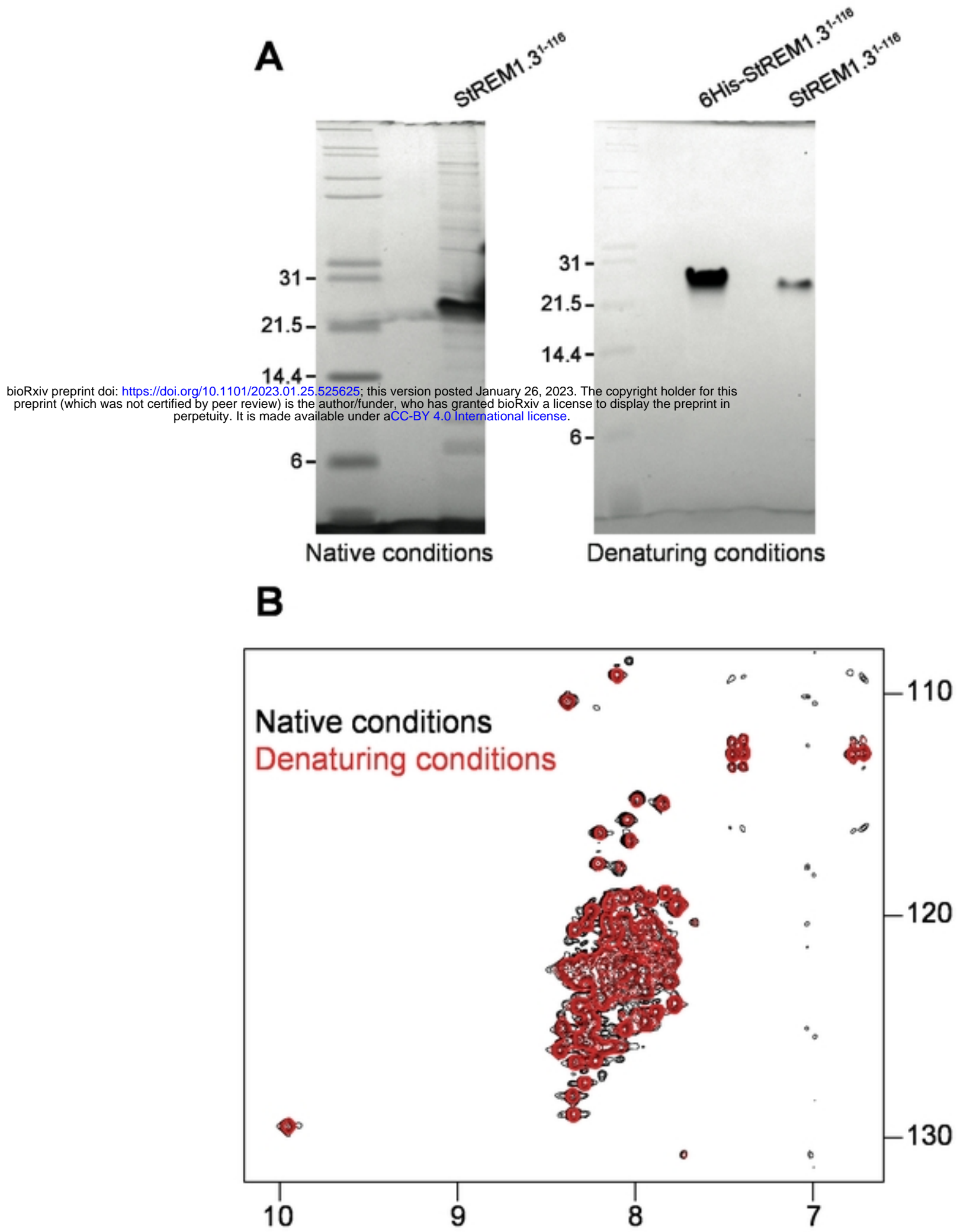


Figure 5 | StADF2 alters StREM1.3 nanodomains to inhibit PVX cell-to-cell movement.



bioRxiv preprint doi: <https://doi.org/10.1101/2023.01.25.525625>; this version posted January 26, 2023. The copyright holder for this preprint (which was not certified by peer review) is the author/funder, who has granted bioRxiv a license to display the preprint in perpetuity. It is made available under a [CC-BY 4.0 International license](https://creativecommons.org/licenses/by/4.0/).

Figure supplemental 1 | StREM1.3 N-terminal domain is intrinsically disordered

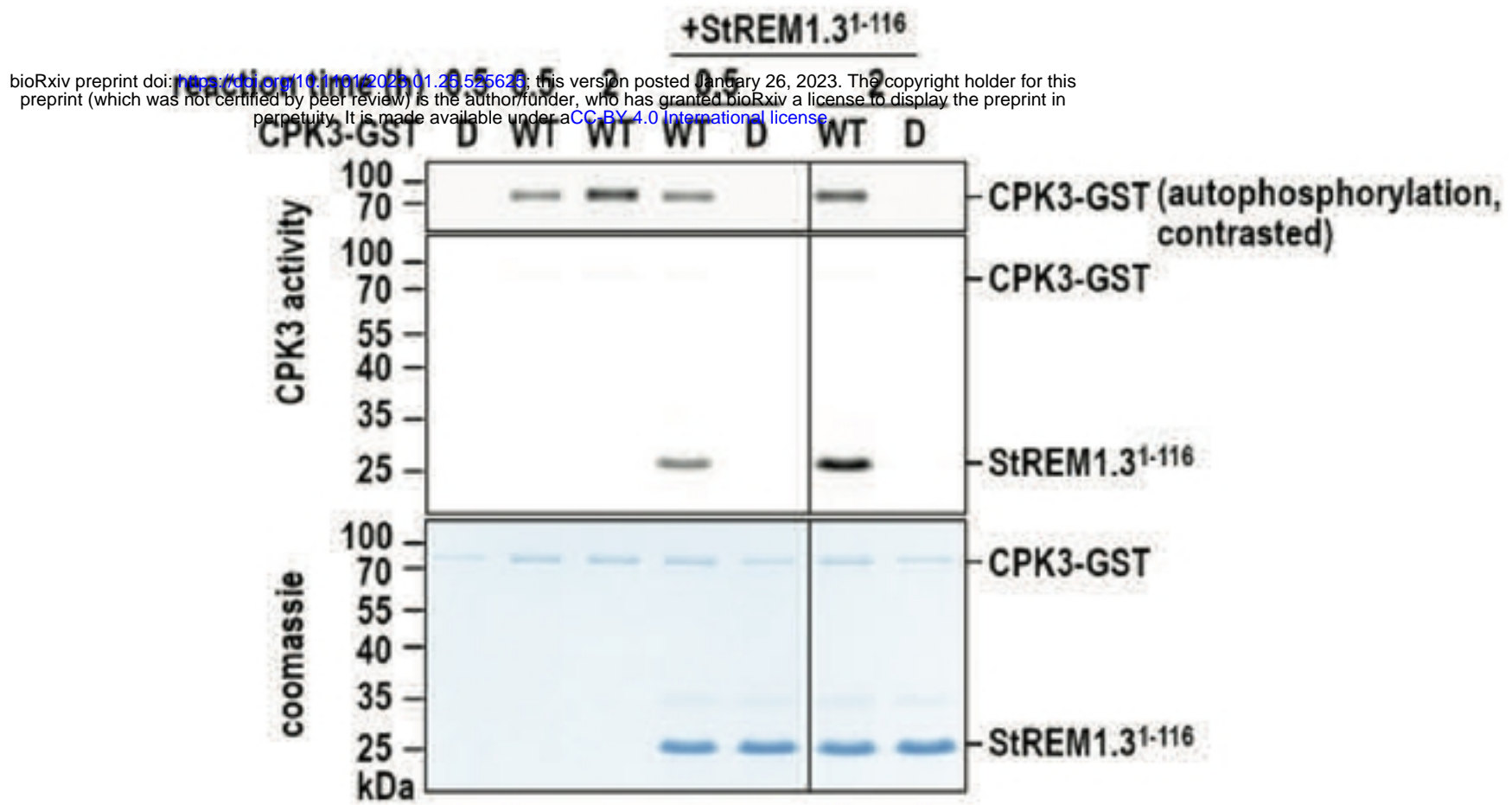


Figure supplemental 2 | AtCPK3 phosphorylates StREM1.3¹⁻¹¹⁶ under NMR conditions.

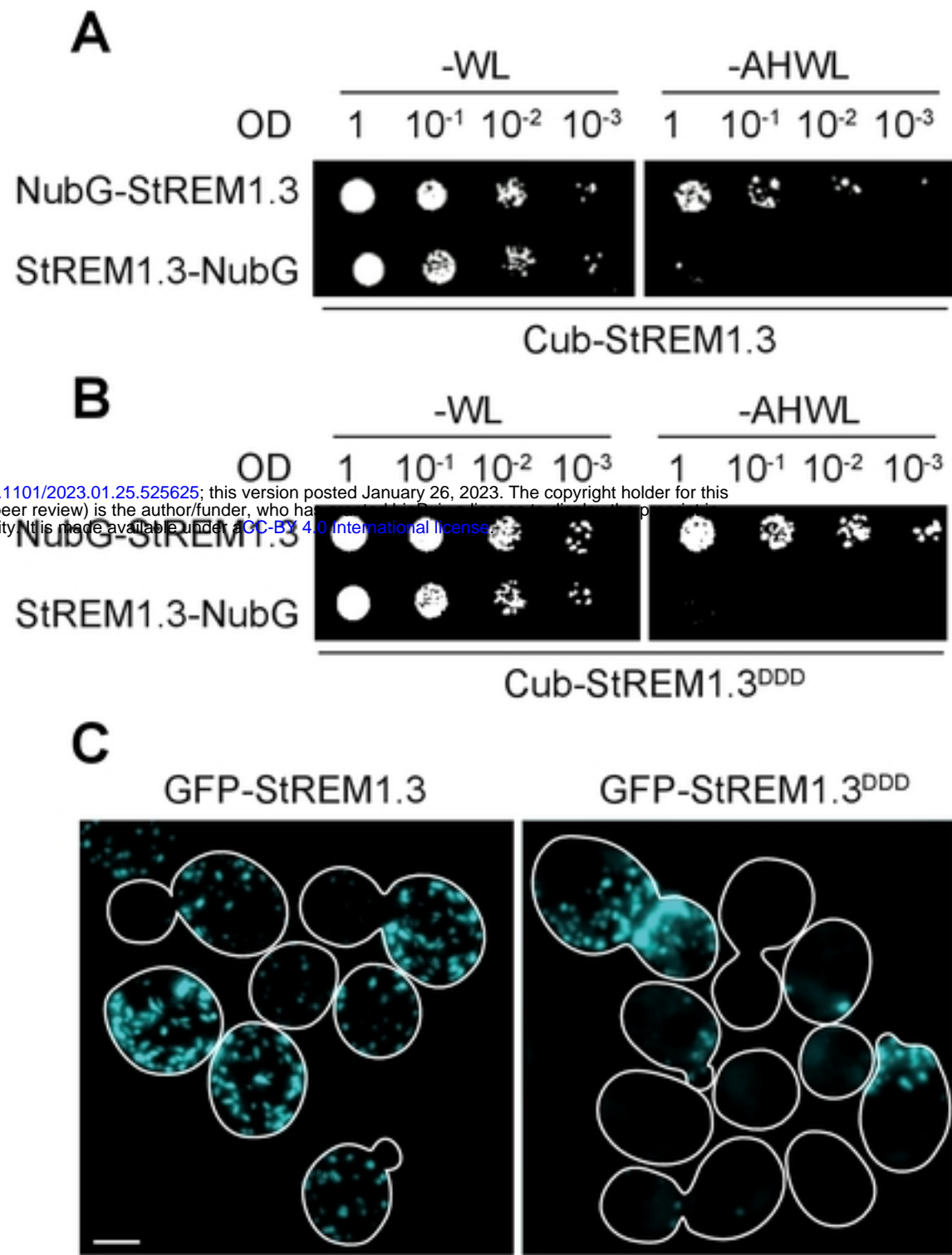
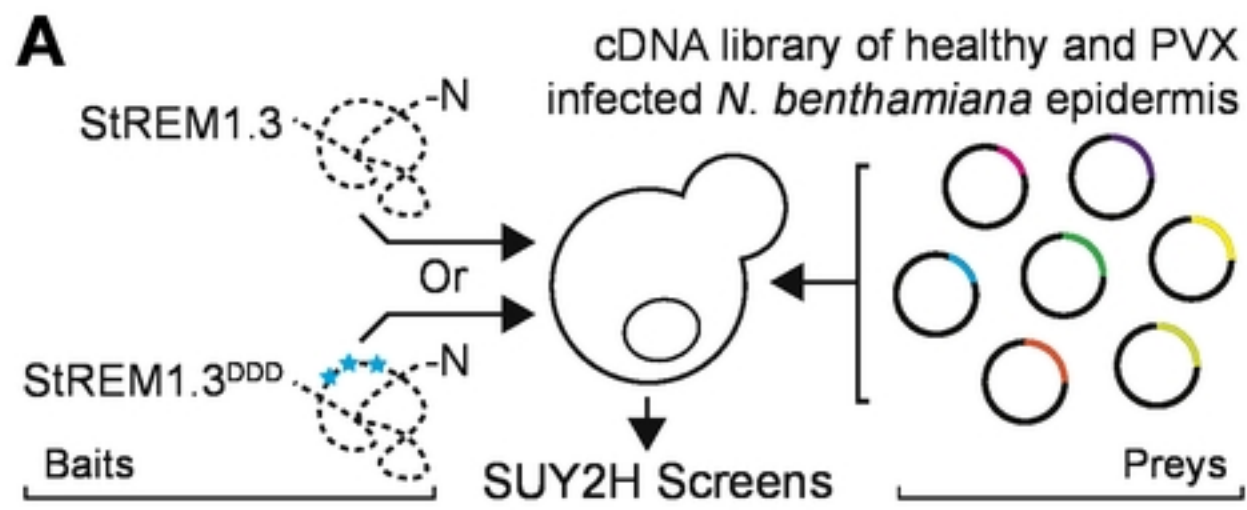


Figure supplemental 3 | Cub-StREM1.3 and Cub-StREM1.3^{DDD} are functional baits in SUY2H.



bioRxiv preprint doi: <https://doi.org/10.1101/2023.01.25.525625>; this version posted January 26, 2023. The copyright holder for this preprint (which was not certified by peer review) is the author/funder, who has granted bioRxiv a license to display the preprint in perpetuity. It is made available under aCC-BY 4.0 International license.

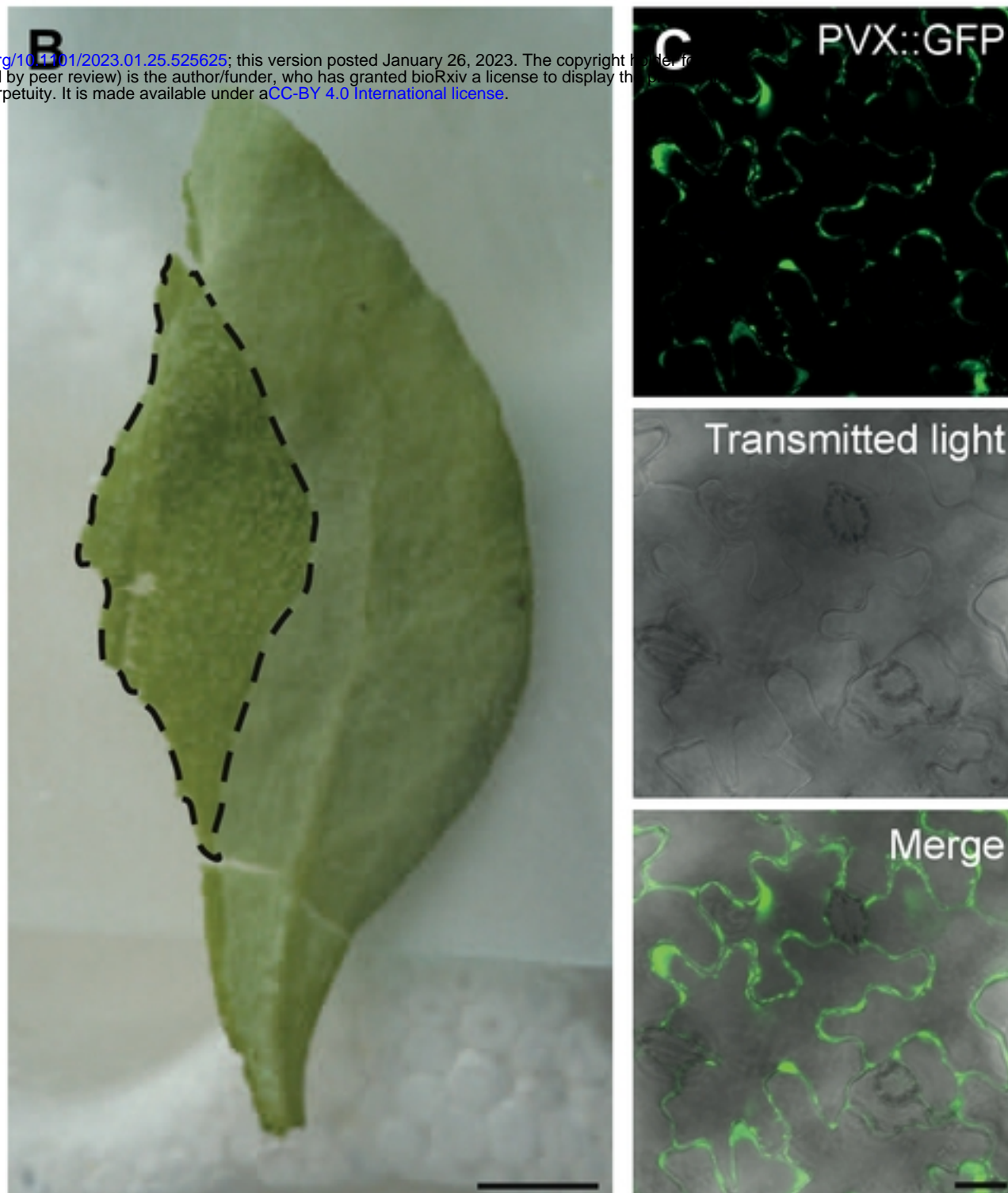


Figure supplemental 4 | Rational design of the SUY2H screens.

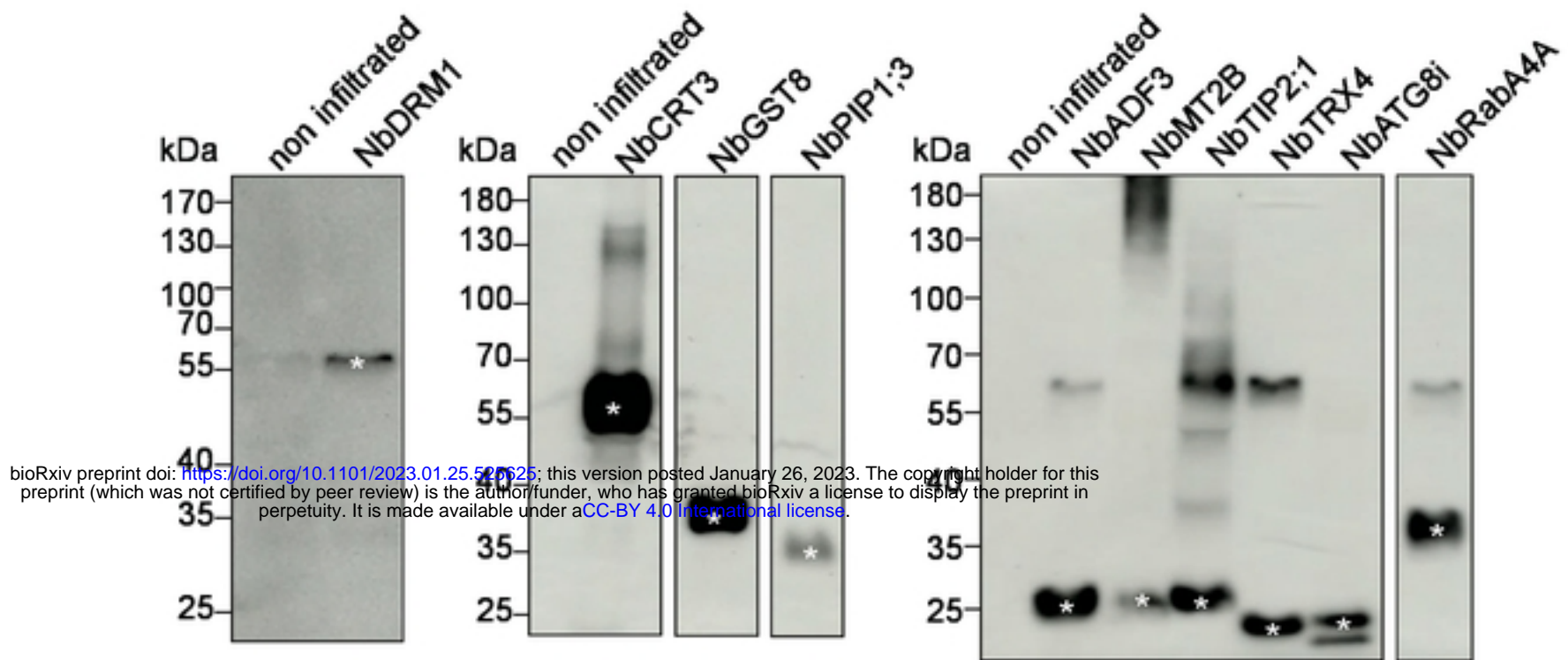


Figure supplemental 5 | Western blots analyses of the expression of protein candidates in PVX cell-to-cell movement assays.

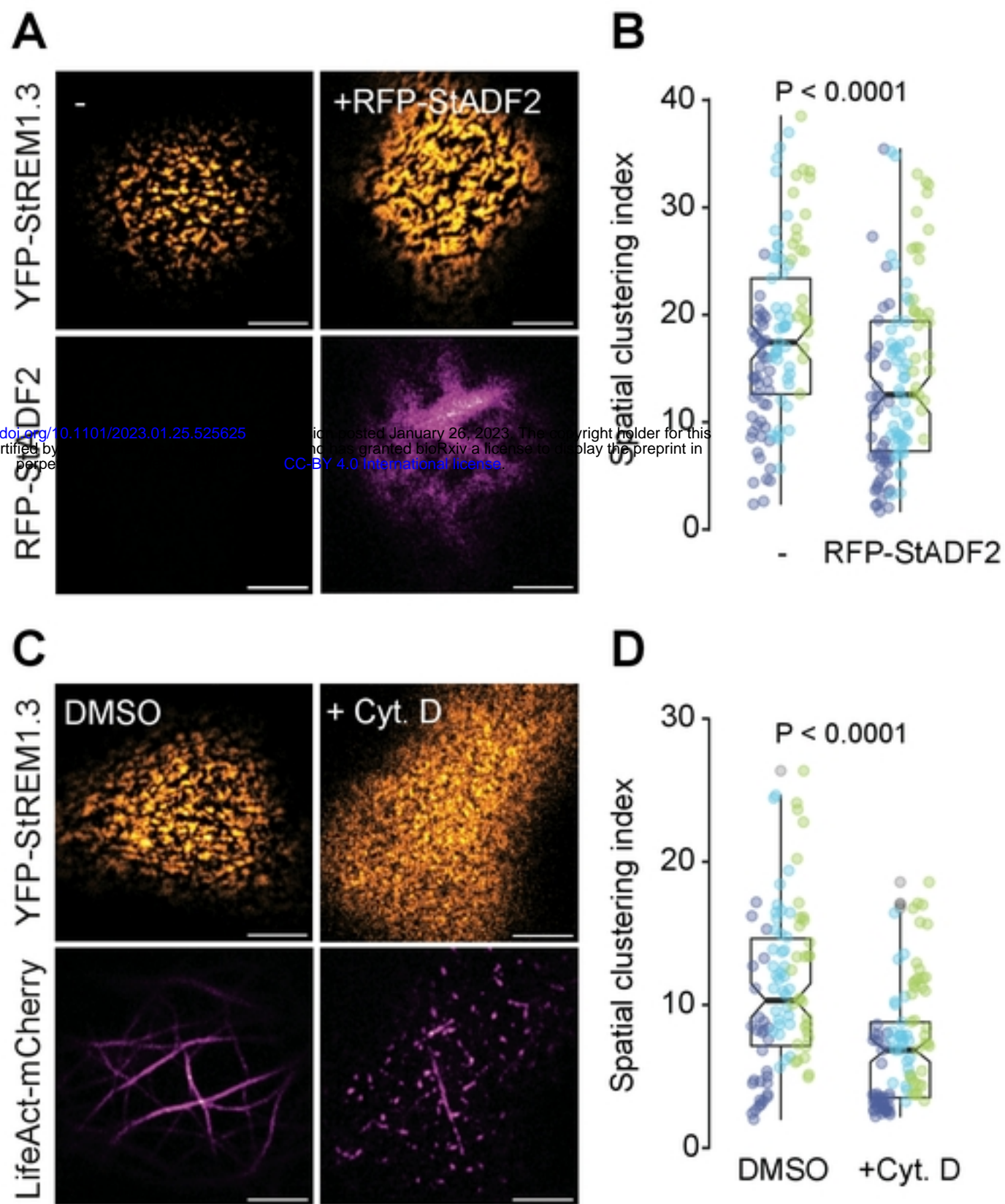


Figure supplemental 6 | StADF2 affects YFP-StREM1.3 nanodomain organization and YFP-StREM1.3 nanodomain rely on the actin cytoskeleton integrity.

bioRxiv preprint doi: <https://doi.org/10.1101/2023.01.25.525625>; this version posted January 26, 2023. The copyright holder for this preprint (which was not certified by peer review) is the author/funder, who has granted bioRxiv a license to display the preprint in perpetuity. It is made available under aCC-BY 4.0 International license.



Figure supplemental 7 | Serine 6 is conserved among ADFs